

Waveform Relaxation for the Computational Homogenization of Multiscale Magnetoquasistatic Problems

I. Niyonzima^{a,b,*}, C. Geuzaine^c, S. Schöps^{a,b}

^a*Institut für Theorie Elektromagnetischer Felder, Technische Universität Darmstadt, Schlossgartenstrasse 8, D-64289 Darmstadt, Germany.*

^b*Graduate School of Computational Engineering, Technische Universität Darmstadt, Dolivostrasse 15, D-64293 Darmstadt, Germany.*

^c*Applied and Computational Electromagnetics (ACE), Université de Liège, Montefiore Institute, Quartier Polytech 1, Allée de la découverte 10, B-4000 Liège, Belgium*

Abstract

This paper proposes the application of the waveform relaxation method to the homogenization of multiscale magnetoquasistatic problems. In the monolithic heterogeneous multiscale method, the nonlinear macroscale problem is solved using the Newton–Raphson scheme. The resolution of many mesoscale problems per Gauß point allows to compute the homogenized constitutive law and its derivative by finite differences. In the proposed approach, the macroscale problem and the mesoscale problems are weakly coupled and solved separately using the finite element method on time intervals for several waveform relaxation iterations. The exchange of information between both problems is still carried out using the heterogeneous multiscale method. However, the partial derivatives can now be evaluated exactly by solving only one mesoscale problem per Gauß point.

Keywords: Cosimulation method, Eddy currents, Finite element method, FE², HMM, Homogenization, Multiscale modeling, Nonlinear problems, Magnetoquasistatic problems, Waveform relaxation method.

1. Introduction

The recent use of the heterogeneous multiscale method (HMM [1]) in electrical engineering has allowed to accurately solve magnetoquasistatic (MQS) problems with multiscale materials, e.g. microstructured composites with ferromagnetic inclusions exhibiting hysteretic magnetic behavior [2, 3]. The method requires the solution of one macroscale and mesoscale problems at each Gauß point of the macroscale problem (see Figure 1) in a coupled formulation based on the Finite Element (FE) method. In [2, 3] the coupled problem was monolithically time discretized by using equal step sizes at all scales and the resulting nonlinear problem was solved by an inexact parallel multilevel Newton-Raphson scheme. The finite-difference approach involves the resolution of 4 mesoscale problems in the three-dimensional case (respectively 3 mesoscale problems in two-dimensions) for computing the approximated Jacobian at each Gauß point.

The use of different time steps becomes important for problems involving different dynamics at both scales. In the case of the soft ferrite material studied in [4], for example, it was shown that capacitive effects occurring at the mesoscale could be accounted for by upscaling proper homogenized quantities in the macroscopic MQS formulation. Another relevant case involves perfectly isolated laminations and soft magnetic composites (SMC) with eddy currents at the mesoscopic level (scales of the sheet/metalic grain) but without the resulting macroscopic eddy currents. The application of the HMM to problems involving such materials leads to a formulation featuring magnetodynamic problems at the mesoscopic scale and a magnetostatic problem at the macroscopic level. Thus, small time steps should be used at the mesoscale to resolve the eddy currents (especially with saturated hysteretic materials) while large time steps could be

*Corresponding author.

**Email addresses: niyonzima@gsc.tu-darmstadt.de (I. Niyonzima), cgeuzaine@ulg.ac.be (C. Geuzaine), schoeps@gsc.tu-darmstadt.de (S. Schöps)

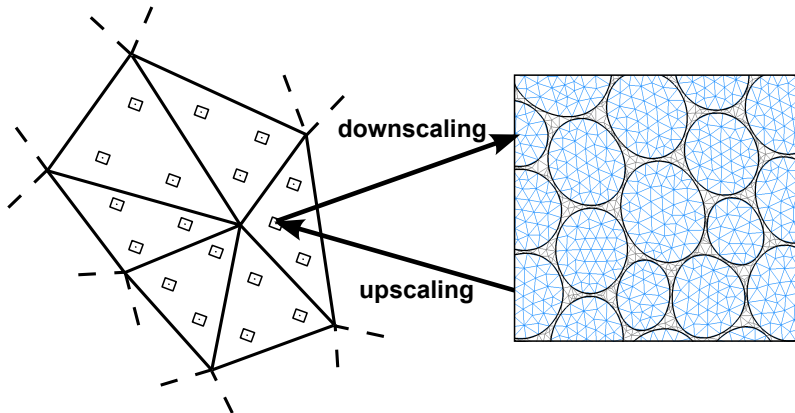


Figure 1: Scale transitions between macroscale (left) and mesoscale (right) problems. Downscaling (Macro to meso): obtaining proper boundary conditions and the source terms for the mesoscale problem from the macroscale solution. Upscaling (meso to Macro): effective quantities for the macroscale problem calculated from the mesoscale solution [2, 3].

used to discretize the rather slowly-varying exciting source current at the macroscale level. Obviously, in such cases of different dynamics, the use of different time steps can help to reduce the overall computational cost.

In this paper we propose a novel approach that provides a natural setting for the use of different time steps. The approach applies the waveform relaxation method [5, 6] to the homogenization of MQS problems: the macroscale problem and the mesoscale problems are solved separately on time intervals and their time-dependent solutions are exchanged in a fixed point iteration. The decoupling of the macroscale and the mesoscale problems and the independent resolution of these problems on time intervals has the potential to significantly reduce both the computation and communication cost of the multiscale scheme; in particular it allows to compute the Jacobian exactly at each Gauß point of the macroscale domain by solving only one mesoscale problem. As a drawback, waveform relaxation iterations are needed for the overall problem to converge in addition to the Newton–Raphson iterations on the meso- and macroscale. The latter exhibits quadratic convergence, while the fixed point iteration only leads to a linear convergence but is applied to waveforms instead of classical vector spaces. We present both approaches and compare the computational and the communication costs for both the monolithic and the waveform relaxation HMM.

The article is organized as follows: in Section 2 we introduce Maxwell’s equations and the MQS problem. The weak form of the MQS problem is then derived using the modified vector potential formulation. Section 3 deals with the multiscale formulations of the HMM for the MQS problem along the lines of the works [2, 3] with an emphasis on the coupling between the macroscale and the mesoscale problems. These formulations are valid for the monolithic and the waveform relaxation (WR) HMM. In Section 4 we develop a novel theoretical framework for the monolithic HMM. Using this framework we derive a reduced Jacobian from the Jacobian of the full problem using the Schur complement, similar as it has been proposed for the Variational Multiscale Method in [4]. Section 5 gives a short overview of the waveform relaxation method. The notion of weak and strong coupling are explained in the general context of coupled systems. The method is then used in Section 6 in combination with the HMM and gives rise to the newly developed WR–HMM. Section 7 is dedicated to the estimation of the computational cost for both the monolithic HMM and the WR–HMM. Formulae for the computation of costs for the monolithic HMM and the WR–HMM are derived and analyzed to give a hint on a possible reduction of the computational cost of both methods. Section 8 deals with an application case. We consider an application involving idealized soft magnetic materials (SMC) without global eddy currents. Convergence of the method as a function of the waveform relaxation iterations and the macroscale/mesoscale time stepping is numerically investigated.

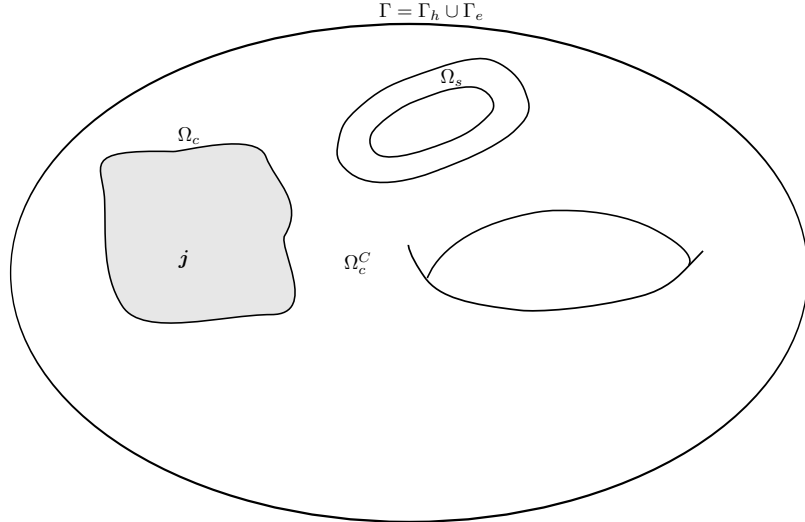


Figure 2: Bounded domain Ω and its subregions [2, 3]. The domain Ω can be split into the conducting region Ω_c (with $\sigma > 0$) and the non-conducting region $\Omega_c^C = \Omega \setminus \Omega_c$ (with $\sigma = 0$) which contains inductors Ω_s where the current density \mathbf{j}_s is imposed. The boundary of the domain Γ is such that $\Gamma = \Gamma_e \cup \Gamma_h$ with $\Gamma_e \cap \Gamma_h = \emptyset$. The region Γ_e is the part of the boundary where the tangential trace of \mathbf{e} (resp. the normal trace of \mathbf{b}) is imposed and Γ_h is the part of the boundary where the tangential trace of \mathbf{h} (resp. the normal trace of \mathbf{d} or \mathbf{j}) is imposed.

2. The magnetoquasistatic problem

In an open, bounded domain $\Omega = \Omega_c \cup \Omega_c^C \subset \mathbb{R}^3$ (see Figure 2) and $t \in \mathcal{I} = (t_0, t_{\text{end}}] \subset \mathbb{R}$, the evolution of electromagnetic fields is governed by the following Maxwell's equations on $\Omega \times \mathcal{I}$, i.e.,

$$\text{curl } \mathbf{h} = \mathbf{j} + \partial_t \mathbf{d}, \quad \text{curl } \mathbf{e} = -\partial_t \mathbf{b}, \quad \text{div } \mathbf{d} = \rho, \quad \text{div } \mathbf{b} = 0,$$

and the constitutive laws, e.g. [7]

$$\mathbf{j}(\mathbf{x}, t) = \mathcal{J}(\mathbf{e}(\mathbf{x}, t), \mathbf{x}), \quad \mathbf{d}(\mathbf{x}, t) = \mathcal{D}(\mathbf{e}(\mathbf{x}, t), \mathbf{x}), \quad \mathbf{h}(\mathbf{x}, t) = \mathcal{H}(\mathbf{b}(\mathbf{x}, t), \mathbf{x}). \quad (2.1 \text{ a-c})$$

In these equations, \mathbf{h} is the magnetic field [A/m], \mathbf{b} the magnetic flux density [T], \mathbf{e} the electric field [V/m], \mathbf{d} the electric flux density [C/m²], \mathbf{j} the electric current density [A/m²], and ρ the electric charge density [C/m³]. The domain Ω_c contains conductors whereas the domain Ω_c^C contains insulators. Additionally, suitable initial conditions and boundary conditions must be imposed for the problem to be well posed.

In this paper we consider only the ‘magnetoquasistatic’ (MQS) case; it is derived from Maxwell's equations by neglecting the displacement currents with respect to the eddy currents $\partial_t \mathbf{d} \ll \mathbf{j}$. This can be justified if $L \ll \lambda$ and $\delta \simeq L$ with L , the characteristic length of the system, λ the wavelength of the exciting source and δ the skin depth. A more rigorous analysis can be found in [8]. The resulting eddy current problem can be defined by the following MQS approximation of Maxwell's equations [9]

$$\text{curl } \mathbf{h} = \mathbf{j}, \quad \text{curl } \mathbf{e} = -\partial_t \mathbf{b}, \quad \text{div } \mathbf{b} = 0, \quad (2.2 \text{ a-c})$$

and the relevant constitutive laws for \mathbf{j} (see equation (2.1 a)) and \mathbf{h} (see equation (2.1 b)). For the applications treated in this paper the first (electric) constitutive law will be considered of the form $\mathbf{j}(\mathbf{x}, t) = \sigma(\mathbf{x}) \mathbf{e}(\mathbf{x}, t) + \mathbf{j}_s(\mathbf{x}, t)$, with σ the (anisotropic) electric conductivity and \mathbf{j}_s an imposed (source) electric current density in $\Omega_s \subset \Omega_c^C$ [A/m²]. The second (magnetic) constitutive law can be linear, nonlinear reversible or nonlinear irreversible (i.e. with hysteresis). Typical nonlinear reversible models include Brauer's model [10], Roug e's formula [11] or splines.

Boundary conditions on the tangential component of the magnetic field (or on the normal component of \mathbf{j}) and on the normal component of the magnetic flux density (or on the tangential component of \mathbf{e})

are imposed on complementary parts Γ_h and Γ_e of the boundary $\Gamma = \partial\Omega = \Gamma_e \cup \Gamma_h$:

$$\mathbf{n} \times \mathbf{h}|_{\Gamma_h} = \mathbf{h}_t, \quad \mathbf{n} \cdot \mathbf{b}|_{\Gamma_e} = b_n. \quad (2.3 \text{ a-b})$$

In this paper, we use the modified vector potential formulation and write \mathbf{b} and \mathbf{e} as:

$$\mathbf{b} = \text{curl } \mathbf{a}, \quad \mathbf{e} = -\partial_t \mathbf{a} \quad (2.4 \text{ a-b})$$

with \mathbf{a} the magnetic vector potential [Vs/m]. Therefore the essential boundary condition $\mathbf{n} \cdot \mathbf{b}|_{\Gamma_e} = \mathbf{n} \cdot (\text{curl } \mathbf{a})|_{\Gamma_e} = b_n$ leads to the cancellation of the normal component of the curl and can be fulfilled by imposing $\mathbf{n} \times \mathbf{a}|_{\Gamma_e} = \mathbf{0}$.

The MQS problem (2.2 a-c) together with the constitutive laws (2.1 a) and (2.1 c) can be solved using the finite element method. To do this, a Galerkin formulation of the problem must be developed. Existence of the (weak) solutions presupposes some regularity assumptions on the data of the problem. The conductivity σ is defined such that the mapping \mathcal{J} defined in (2.1 a) is monotone, nondecreasing and continuous in \mathbf{e} . For the linear electric law used in this paper, these conditions are fulfilled if σ is bounded, i.e., if $\sigma \in L^\infty(\Omega)$. The mapping \mathcal{H} is assumed to be maximal monotone which presupposes that $\partial\mathcal{H}/\partial\mathbf{b}$ is positive definite. This is the case for linear and nonlinear magnetic mappings but does not hold for hysteretic magnetic materials. The excitation term \mathbf{j}_s needs also to be regular enough, e.g., $\mathbf{j}_s \in L^2((0, T); V(\Omega)^*)$. The space $V(\Omega) := \mathbf{H}_e(\text{curl}; \Omega)$ is the appropriate function space for the vector potential with boundary conditions on Γ_e , and the superscript $*$ is used to denote its dual (see [9, 12]).

Using these assumptions, the weak form of (2.2 a) reads [12, 13]: find $\mathbf{a} \in L^2((0, T); V(\Omega))$ with $\partial_t \mathbf{a} \in L^2((0, T); V(\Omega)^*)$ such that

$$(\sigma \partial_t \mathbf{a}, \mathbf{a}')_{\Omega_e} + (\mathcal{H}(\text{curl } \mathbf{a}), \text{curl } \mathbf{a}')_{\Omega} + \langle \mathbf{h}_t, \mathbf{a}' \rangle_{\Gamma_h} - (\mathbf{j}_s, \mathbf{a}')_{\Omega_s} = 0 \quad (2.5)$$

holds for all test functions $\mathbf{a}' \in V_0(\Omega)$, where the subscript $_0$ is used to denote homogeneous boundary Dirichlet conditions. More regularity in time and space for the solution can be obtained by imposing more regularity on the data of the problem [14] Round brackets (\cdot, \cdot) are used for volume integrals whereas angle brackets $\langle \cdot, \cdot \rangle$ are used for surface integrals. The field \mathbf{a} derived from (2.5) must be gauged on Ω_c^C to ensure its uniqueness. This can mathematically be achieved by factoring the space $\mathbf{H}_e^0(\text{curl}; \Omega)$ by gradients of scalar potentials, e.g., [12].

2.1. Multiscale

Following [2, 3, 15], we use the subscript $\varepsilon = l/L$ to denote quantities with rapid fluctuations. The length l denotes the length of the periodic cell and the length L denotes the characteristic length of the material or the minimum wavelength of the exciting source current $\mathbf{j}_s(t)$. This wavelength is defined as $\lambda_{\min} = c/f_{\max}$ where c is the speed of light and f_{\max} is the highest frequency obtained when $\mathbf{j}_s(t)$ is decomposed using the Fourier transform. The homogenized computational domain is assumed to be located far from the boundary Γ such that the boundary term in (2.5) is independent of ε . Using this convention we can define the equivalent multiscale weak form for equation (2.5).

Problem 2.1 (Multiscale finescale problem). *Find $\mathbf{a}^\varepsilon \in L^2((0, T); V(\Omega))$ with $\partial_t \mathbf{a}^\varepsilon \in L^2((0, T); V(\Omega)^*)$ such that*

$$(\sigma^\varepsilon \partial_t \mathbf{a}^\varepsilon, \mathbf{a}'^\varepsilon)_{\Omega_c} + (\mathcal{H}^\varepsilon(\text{curl } \mathbf{a}^\varepsilon), \text{curl } \mathbf{a}'^\varepsilon)_{\Omega} + \langle \mathbf{h}_t, \mathbf{a}'^\varepsilon \rangle_{\Gamma_h} - (\mathbf{j}_s, \mathbf{a}'^\varepsilon)_{\Omega_s} = 0 \quad (2.6)$$

holds for all test functions $\mathbf{a}'^\varepsilon \in V_0(\Omega)$.

This ‘finescale’ weak form is used as the reference solution for problems involving multiscale materials. The conductivity σ^ε and the material mapping \mathcal{H}^ε are defined by

$$\sigma^\varepsilon(\mathbf{x}) = \sigma\left(\frac{\mathbf{x}}{\varepsilon}\right) \quad \text{and} \quad \mathcal{H}^\varepsilon(\mathbf{b}^\varepsilon(\mathbf{x}, t), \mathbf{x}) = \overline{\mathcal{H}}(\mathbf{b}^\varepsilon(\mathbf{x}, t), \mathbf{x}, \mathbf{x}/\varepsilon) \quad (2.7)$$

for all $\mathbf{x} = (x_1, x_2, x_3)$ in Ω_H , where Ω_H is the multiscale computational domain. The mapping $\overline{\mathcal{H}}$ is used to represent two-scale composite materials for which the characteristic length at the mesoscale is ε [15]. By abuse of notation, we use \mathcal{H} instead of $\overline{\mathcal{H}}$ in the rest of the text. In (2.7), slow variations of the

material law are accounted for by the term \mathbf{x} while the fast fluctuations are accounted for by the term \mathbf{x}/ε for $\varepsilon \ll 1$ (see [16, 17, 15]).

As an illustration, consider a two-dimensional linear magnetic material law $\mathcal{H}(\mathbf{b}(\mathbf{x}, t), \mathbf{x}) = \mu(\mathbf{x}) \mathbf{b}(\mathbf{x}, t)$ with the magnetic permeability defined as

$$\mu(\mathbf{x}) = \begin{cases} \mu_1 & \text{if } (x_1 \bmod T) \leq \lambda, \\ \mu_2 & \text{if } (x_1 \bmod T) > \lambda, \end{cases}$$

for all $\mathbf{x} \in \Omega_H$, positive μ_1, μ_2 and $\lambda < T$. The magnetic permeability μ is periodic with period T and is representative of a stack of laminations made of two materials. The division by the parameter ε allows to make the period smaller (from T to εT). In the previous case, the permeability becomes:

$$\mu(\mathbf{x}/\varepsilon) = \begin{cases} \mu_1 & \text{if } (\mathbf{x} \bmod \varepsilon T) \leq \lambda, \\ \mu_2 & \text{if } (\mathbf{x} \bmod \varepsilon T) > \lambda, \end{cases}$$

and is ε -periodic. Therefore the material law $\mathcal{H}^\varepsilon(\mathbf{b}^\varepsilon(\mathbf{x}, t), \mathbf{x}, \mathbf{x}/\varepsilon) = \mu(\mathbf{x}/\varepsilon) \mathbf{b}^\varepsilon(\mathbf{x}, t)$ is rapidly fluctuating for $\varepsilon \ll 1$.

In the following sections, the indices M, m and c are used for denoting the macroscale, the mesoscale and correction terms, respectively. The variables $\mathbf{x} \in \Omega$ and $\mathbf{y} = (y_1, y_2, y_3) \in \Omega_m$ are the macroscale and the mesoscale coordinates and the mesoscale coordinates are only defined on the cell domain with the origin at the barycenter.

3. The heterogeneous multiscale method

Developments of this section are derived along the lines of ideas in [2, 3]. The resolution of the finescale reference Problem 2.1 is computationally expensive for small values of ε . Hence, multiscale methods as HMM [1] are necessary to reduce the computational costs and eventually make realistic simulations feasible.

For the MQS problems, HMM is based on the scale separation assumption ($\varepsilon \ll 1$) and was already illustrated in Figure 1. When HMM is applied, the finescale problem is replaced by one macroscale problem defined on a coarse mesh covering the entire domain and accounting for the slow variations of the finescale solution, and by many mesoscale problems defined on small, finely meshed areas around some points of interest of the macroscale mesh (e.g. numerical quadrature points), and are used for computing missing information. The transfer of information between these problems is done during the *upscaling* and the *downscaling* stages.

Equations governing the macroscale and the mesoscale are derived from the finescale problem using the asymptotic homogenization theories. The macroscale problem is derived from the finescale problem using the classical weak convergence theory whereas the mesoscale problem is derived using the two-scale convergence [15]. For these convergence theories to be applied, the solution of the finescale Problem 2.1 must exist and belong to appropriate function spaces (e.g.: reflexive or separable Banach spaces). This imposes some regularity conditions on σ^ε , \mathcal{H}^ε and on the excitation \mathbf{j}_s which have been stated in Section 2. However, the HMM has been numerically used for hysteretic magnetic laws that do not fulfill the monotonicity assumptions on \mathcal{H}^ε [3].

3.1. The macroscale problem

The macroscale weak form of the problem in \mathbf{a} -formulation can be derived from equation (2.5) as follows [3]:

Problem 3.1 (Macroscale weak problem). *Find $\mathbf{a}_M \in L^2((0, T); V(\Omega))$ with $\partial_t \mathbf{a}_M \in L^2((0, T); V(\Omega)^*)$ such that*

$$\left(\sigma_M \partial_t \mathbf{a}_M, \mathbf{a}'_M \right)_{\Omega_c} + \left(\mathcal{H}_M(\mathbf{b}_M, \mathbf{x}), \text{curl}_{\mathbf{x}} \mathbf{a}'_M \right)_{\Omega} + \left\langle \mathbf{n} \times \mathbf{h}_M, \mathbf{a}'_M \right\rangle_{\Gamma_h} - \left(\mathbf{j}_s, \mathbf{a}'_M \right)_{\Omega_s} = 0 \quad (3.1)$$

holds for all $\mathbf{a}'_M \in V_0(\Omega)$, $\mathbf{b}_M := \text{curl}_{\mathbf{x}} \mathbf{a}_M$ and $t \in \mathcal{I} = (t_0, t_{\text{end}}]$.

Thanks to the linearity of the electric law, the macroscopic conductivity σ_M is obtained using the asymptotic expansion method [16]

$$(\sigma_M)_{ij} = \frac{1}{|\Omega_m|} \int_{\Omega_m} \left(\sigma_{ij} - \sum_k \sigma_{ik} \frac{\partial \chi^j(\mathbf{y})}{\partial y_k} \right) d\mathbf{y}, \quad (3.2)$$

where χ^j is obtained by solving the cell problem: find $\chi^j \in V_G$ such that

$$\left((\text{grad}_y \psi)^T, \sigma(\text{grad}_y \chi^j - \mathbf{e}_j) \right)_{\Omega_m} = 0, \quad \forall \psi \in V_G. \quad (3.3)$$

The space V_G is the space $H^1(\Omega_m)$ with periodic boundary conditions while \mathbf{e}_j is the unit vector in the j^{th} spatial direction. The field $\mathbf{b}_c = \text{curl}_y \mathbf{a}_c$ is the magnetic correction field obtained by solving the mesoscale problem corresponding to points $\mathbf{x} \in \Omega$. The mesoscale fields depend on the associated macroscale field and vice versa due to coupling of scales, i.e.,

$$\mathbf{a}_c(\mathbf{x}, \mathbf{y}, t) = \mathcal{A}_c(\mathbf{y}, \mathbf{a}_M(\mathbf{x}, t)) \quad (3.4)$$

where \mathcal{A}_c denotes the solution operator of the mesoscale problem to be described in the following section 3.2. It is defined in analogy to the corrector operator defined in [18] for nonlinear scalar elliptic problems. The macroscopic magnetic law \mathcal{H}_M in (3.1) is computed at each point $(\mathbf{x}, t) \in \Omega \times \mathcal{I}$ using both scales according to the averaging formula from the two-scale convergence theory [15]

$$\mathcal{H}_M(\mathbf{b}_M(\mathbf{x}, t), \mathbf{x}) := \frac{1}{|\Omega_m|} \int_{\Omega_m} \mathcal{H}(\mathbf{b}_c(\mathbf{x}, \mathbf{y}, t) + \mathbf{b}_M(\mathbf{x}, t), \mathbf{x}, \mathbf{y}) d\mathbf{y} \quad \forall (\mathbf{x}, t) \in \Omega \times \mathcal{I} \quad (3.5)$$

where $\mathbf{b}_M := \text{curl}_x \mathbf{a}_M$ and $\mathbf{b}_c = \text{curl}_y \mathcal{A}_c(\mathbf{y}, \mathbf{a}_M)$. The underlying constitutive law \mathcal{H} is known for the heterogeneous phases at the mesoscale level.

3.2. Mesoscale problems

The following weak form of the mesoscale is defined from equation (2.5) [15, 3]

Problem 3.2 (Mesoscale weak problem). *Find the mesoscale correction $\mathbf{a}_c \in L^2((0, T); V_{\text{per}}(\Omega_m))$ with $\partial_t \mathbf{a}_c \in L^2((0, T); V_{\text{per}}(\Omega_m)^*)$ using periodic boundary conditions such that*

$$\left(\sigma \partial_t \mathbf{a}_c, \mathbf{a}'_c \right)_{\Omega_{\text{mc}}} + \left(\mathcal{H}(\mathbf{b}_c + \mathbf{b}_M, \mathbf{x}, \mathbf{y}), \text{curl}_y \mathbf{a}'_c \right)_{\Omega_m} - \left(\sigma \mathbf{e}_M, \mathbf{a}'_c \right)_{\Omega_{\text{mc}}} = 0, \quad (3.6)$$

for all $\mathbf{a}'_c \in V_{\text{per}}(\Omega_m)$, magnetic correction field $\mathbf{b}_c = \text{curl}_y \mathbf{a}_c$, and periodic boundary conditions and \mathbf{b}_M given. The subscript $_{\text{per}}$ is used to denote the use of periodic boundary conditions.

The macroscale magnetic and electric fields are defined as

$$\begin{aligned} \mathbf{b}_M(\mathbf{x}, t) &:= \text{curl}_x \mathbf{a}_M(\mathbf{x}, t) \\ \mathbf{e}_M(\mathbf{x}, t) &:= -\partial_t \mathbf{a}_M(\mathbf{x}, t) - \kappa(\partial_t \mathbf{b}_M \times \mathbf{y})^T \end{aligned}$$

with $\kappa = 1$ for two-dimensional problems and $\kappa = 1/2$ for three-dimensional problems. Existence and uniqueness of the mesoscale correction \mathbf{a}_c motivates the introduction of the solution operator in (3.4). It can be formally deduced based on standard theory for nonlinear elliptic-parabolic problems, e.g. [12, 19, 20, 21].

3.3. Space and time discretization

Macroscale and mesoscale equations are solved using the finite element method. The first step consists in discretizing the computational domain into elements. The fields \mathbf{a}_M^H and \mathbf{a}_c^h are approximation of the continuous fields \mathbf{a}_M and \mathbf{a}_c on the discretized computational domain and $\mathbf{a}_M^H \in (0, T] \times \mathbf{W}_{H,0}^M$ and

$\mathbf{a}_c^h \in (0, T] \times \mathbf{W}_{h,0}^m$ where $\mathbf{W}_{H,0}^M$ and $\mathbf{W}_{h,0}^m$ are $H(\text{curl})$ -conforming edge finite elements. In this paper we consider only lowest order $H(\text{curl})$ -conforming edge finite elements as test and basis functions, i.e.,

$$\begin{aligned}\mathbf{W}_{H,0}^M &:= \left\{ \mathbf{v} \in \mathbf{H}(\text{curl}; \Omega) \mid \mathbf{v} \in \mathcal{N}_0^I(K_M) \forall K_M \in \mathcal{T}_H^M \right\}, \\ \mathbf{W}_{h,0}^m &:= \left\{ \mathbf{v} \in \mathbf{H}(\text{curl}; \Omega_m) \mid \mathbf{v} \in \mathcal{N}_0^I(K_m), \forall K_m \in \mathcal{T}_h^m \right\}\end{aligned}\quad (3.7)$$

where $\mathcal{N}_0^I(K) := \{ \mathbf{a} + \mathbf{b} \times \mathbf{x} \mid \mathbf{a}, \mathbf{b} \in \mathbb{R}^3 \}$, see e.g. [9]. The triangulations \mathcal{T}_H^M and \mathcal{T}_h^m are defined on the macroscale and mesoscale domains, respectively.

The weak forms (3.1) and (3.6) can then be computed using numerical quadrature rules. This implies that the quantities involved in the integrations (e.g. the homogenized material law) be known at Gauß points ($i = 1, \dots, N_{\text{GP}}$). Omitting the superscript i used for the numbering of the Gauß in the approximation of the mesoscale field $\mathbf{a}_c^h(\mathbf{y}, t)$, the discrete spaces give rise to the approximations

$$\mathbf{a}_M(\mathbf{x}, t) \approx \mathbf{a}_M^H(\mathbf{x}, t) = \sum_{p=1}^{N_M} \alpha_{M,p}(t) \mathbf{a}_{M,p}(\mathbf{x}) \quad \text{and} \quad \mathbf{a}_c^{(i)}(\mathbf{y}, t) \approx \mathbf{a}_c^h(\mathbf{y}, t) = \sum_{p=1}^{N_c} \alpha_{c,p}(t) \mathbf{a}_{c,p}(\mathbf{y}). \quad (3.8)$$

Testing (3.1) and (3.6) yields the macroscale mass matrix

$$\mathbf{M}_M := \left(\sigma_M \mathbf{a}_M, \mathbf{a}'_M \right)_{\Omega_c}$$

which is singular due to $\sigma_M = 0$ on Ω_c^C and the stiffness term

$$\mathcal{F}_M(\alpha_M, \alpha_c) := \left(\mathcal{H}_M(\text{curl}_y \mathbf{a}_c + \text{curl}_x \mathbf{a}_M, \mathbf{x}), \text{curl}_x \mathbf{a}'_M \right)_{\Omega} + \left\langle \mathbf{h}_t, \mathbf{a}'_M \right\rangle_{\Gamma_h} - \left(\mathbf{j}_s, \mathbf{a}'_M \right)_{\Omega_s} \quad (3.9)$$

with $\alpha_c = [\alpha_c^{(1)}, \dots, \alpha_c^{(N_{\text{GP}})}]$. Similar definitions hold for \mathbf{M}_m and \mathcal{F}_m on the mesoscale. The extension to higher order edge elements or nodal elements for 2D problems is straightforward. Following the classical approach, numerical quadrature rules are used to compute the weak forms. For the macroscale problem, we use numerical quadrature with one Gauß point which is enough to capture the slow variations of the missing material law at Gauß points. The missing material law can also be computed at the barycenter of the element [22].

Problem 3.3 (Semidiscrete multiscale problem). *Find waveforms $[\alpha_M(t), \alpha_c^{(1)}(t), \dots, \alpha_c^{(N_{\text{GP}})}(t)]$ such that*

$$\mathbf{M}_M \partial_t \alpha_M + \mathcal{F}_M(\alpha_M, \alpha_c) = 0, \quad (3.10)$$

and for the mesoscale problems $i = 1, \dots, N_{\text{GP}}$

$$\mathbf{M}_m \partial_t \alpha_c^{(i)} + \mathcal{F}_m(\alpha_c^{(i)}, \alpha_M^{(i)}, \partial_t \alpha_M^{(i)}) = 0 \quad (3.11)$$

for a given set of initial values $[\alpha_M(t_0), \alpha_c^{(1)}(t_0), \dots, \alpha_c^{(N_{\text{GP}})}(t_0)]$.

Finally, the time-dependent Problem (3.10-3.11) can be solved using any classical (implicit) time integration scheme followed by a nonlinear solution method. In the simplest case, i.e., using the backward Euler scheme, the following nonlinear problem has to be solved for for each time step:

Problem 3.4 (Nonlinear, discrete multiscale problem). *Find the solutions*

$$[\alpha_M^{(k)}, \alpha_c^{(1,k)}, \dots, \alpha_c^{(N_{\text{GP}},k)}] \in \mathbb{R}^{N_M + N_{\text{GP}} \cdot N_c}$$

such that

$$\mathcal{R}_M \left(\alpha_M^{(k)}, \alpha_c^{(i,k)} \right) := \mathbf{M}_M \frac{\alpha_M^{(k)} - \alpha_M^{(k-1)}}{\Delta t_k} + \mathcal{F}_M \left(\alpha_M^{(k)}, \alpha_c^{(k)} \right) = 0, \quad (3.12)$$

and for the mesoscale problems $i = 1, \dots, N_{\text{GP}}$

$$\mathcal{R}_m \left(\boldsymbol{\alpha}_M^{(k)}, \boldsymbol{\alpha}_c^{(i,k)} \right) := M_m \frac{\boldsymbol{\alpha}_c^{(i,k)} - \boldsymbol{\alpha}_c^{(i,k-1)}}{\Delta t_k} + \mathcal{F}_m \left(\boldsymbol{\alpha}_c^{(i,k)}, \boldsymbol{\alpha}_M^{(i,k)}, \frac{\boldsymbol{\alpha}_M^{(i,k)} - \boldsymbol{\alpha}_M^{(i,k-1)}}{\Delta t_k} \right) = 0, \quad (3.13)$$

where the superscript k is used to denote the approximations at time instants $t_k \in [t_0, t_{\text{end}}]$, e.g. $\boldsymbol{\alpha}_M^{(k)} \approx \boldsymbol{\alpha}_M(t_k)$ and $\Delta t_k := t_{k+1} - t_k$ is the corresponding time step size.

The following loops are defined for the monolithic and the waveform relaxation methods: the loop for the number of time windows (TW) with $1 \leq n \leq N_{\text{TW}}$, the loop for the number of waveform relaxation iterations (WR) with $1 \leq l \leq N_{\text{WR}}$, the loop for the number of time stepping (TS) with $1 \leq k \leq N_{\text{TS}}$, the loop for the number of Newton–Raphson nonlinear iterations (NR) with $1 \leq j \leq N_{\text{NR}}$ and the loop for the number of Gauß points (GP) with $1 \leq i \leq N_{\text{GP}}$. Table 1 summarizes the loops, the letter used for indexing them and the total number of iterations for each loop.

Table 1: Loops involved in the monolithic and waveform relaxation HMM.

Type of loop	Loop	Index	Maximum number of iterations
Time window	TW	n	N_{TW}
Waveform relaxation	WR	l	N_{WR}
Time stepping	TS	k	N_{TS}
Newton–Raphson	NR	j	N_{NR}
Gauß points	GP	i	N_{GP}

4. Monolithic HMM

In the following a rigorous interpretation of the time-stepping procedures proposed in the context of HMM is given in terms of Problem 3.4. These derivations are an important building block for the comparison with the waveform relaxation approach in Section 5.

In [3] the Algorithm 1 was proposed. For each time step, a nonlinear system on the macroscale is solved using the Newton–Raphson method until convergence is reached. In each Newton iteration the material law (3.5) is evaluated

$$\mathcal{H}_M^{(i,j,k)} := \frac{1}{|\Omega_m|} \int_{\Omega_m} \mathcal{H} \left(\mathbf{b}_c^{(i,j,k)}, \text{curl}_x \mathbf{a}_M^{(j,k)}, \mathbf{x}, \mathbf{y} \right) d\mathbf{y}$$

where $\mathbf{b}_c^{(i,j,k)} = \text{curl}_y \mathcal{A}_c(\mathbf{y}, \mathbf{a}_M^{(j,k)})$ is obtained from the discretized version of the nonlinear solution operator given in (3.4). This is implemented by solving the nonlinear equation (3.13) again by the Newton–Raphson method using N_{NR}^m iterations, cf. Algorithm 2. This relaxation within the Newton scheme corresponds to a monolithic time-stepping scheme although it features parallel evaluations at the Gauß points at the level of the nonlinear solver. The two nested new Newton loops (inner and outer) are a special case of a *parallel multilevel Newton scheme* as they are used for example in circuit simulation [23]. Let us state the equivalence for the case in which only one inner iteration of a simplified Newton–Raphson scheme is carried out. This is closely related to the Newton–Raphson scheme developed in [18] which involves the evaluation of the Fréchet derivative of the nonlinear corrector operator.

Let $\boldsymbol{\alpha}_M^{(j,k)}$ and $\boldsymbol{\alpha}_c^{(i,j,k)}$ denote the j^{th} Newton–Raphson iterates. Then we define

$$\mathcal{F}_M^{(j,k)} := \mathcal{F}_M \left(\boldsymbol{\alpha}_M^{(j,k)}, \boldsymbol{\alpha}_c^{(j,k)} \right) \quad , \quad \mathcal{F}_m^{(i,j,k)} := \mathcal{F}_m \left(\boldsymbol{\alpha}_c^{(i,j,k)}, \boldsymbol{\alpha}_M^{(i,j,k)}, \frac{\boldsymbol{\alpha}_M^{(i,j,k)} - \boldsymbol{\alpha}_M^{(i,j,k-1)}}{\Delta t_k} \right). \quad (4.1)$$

Proposition 4.1. *Solving the monolithic system (3.12)-(3.13) with the Newton–Raphson scheme using the Jacobian*

$$J_{\mathcal{R}}^{(j,k)} := \frac{1}{\Delta t_k} \begin{pmatrix} M_M & 0 & \cdots & 0 \\ 0 & M_m & 0 & 0 \\ \vdots & 0 & \ddots & 0 \\ 0 & 0 & 0 & M_m \end{pmatrix} + \begin{pmatrix} \frac{\partial \mathcal{F}_M^{(j,k)}}{\partial \alpha_M^{(j,k)}} & \frac{\partial \mathcal{F}_M^{(j,k)}}{\partial \alpha_c^{(1,j,k)}} & \cdots & \frac{\partial \mathcal{F}_M^{(j,k)}}{\partial \alpha_c^{(N_{GP},j,k)}} \\ \frac{\partial \mathcal{F}_m^{(1,j,k)}}{\partial \alpha_M^{(j,k)}} & \frac{\partial \mathcal{F}_m^{(1,j,k)}}{\partial \alpha_c^{(1,j,k)}} & 0 & 0 \\ \vdots & 0 & \ddots & 0 \\ \frac{\partial \mathcal{F}_m^{(N_{GP},j,k)}}{\partial \alpha_M^{(j,k)}} & 0 & 0 & \frac{\partial \mathcal{F}_m^{(N_{GP},j,k)}}{\partial \alpha_c^{(N_{GP},j,k)}} \end{pmatrix} \quad (4.2)$$

is equivalent to the scheme proposed in Algorithms 1 and 2 if

(a) no inner Newton iterations on the mesoscale are carried out, i.e., $N_{NR}^m = 1$ and

(b) the sensitivity of the mesoscale Jacobian w.r.t. to the macroscale is disregarded, i.e., $\partial J_m^{(i,j,k)} / \partial \alpha_M^{(j,k)} = 0$

Proof. The equivalence is easily established by comparing the solution operator \mathcal{A}_c as used in Algorithms 1-2 to the Schur complement of the Jacobian $J_{\mathcal{R}}^{(j,k)}$ as given in (4.2) and already proposed in [4] for the Variational Multiscale Method. The latter reads

$$\bar{J}_{\mathcal{R}}^{(j,k)} := \frac{M_M}{\Delta t_k} + \frac{\partial \mathcal{F}_M^{(j,k)}}{\partial \alpha_M^{(j,k)}} - \sum_{i=1}^{N_{GP}} \left(\frac{\partial \mathcal{F}_M^{(j,k)}}{\partial \alpha_c^{(i,j,k)}} \left(\frac{M_m}{\Delta t_k} + \frac{\partial \mathcal{F}_m^{(i,j,k)}}{\partial \alpha_c^{(i,j,k)}} \right)^{-1} \frac{\partial \mathcal{F}_m^{(i,j,k)}}{\partial \alpha_M^{(j,k)}} \right). \quad (4.3)$$

Since Assumption (a), i.e., $N_{NR}^m = 1$ in Algorithm 2 holds, the discretized version of the solution operator \mathcal{A}_c applied to the linearized problem (3.13) can be explicitly given as

$$\alpha_c^{(i,j+1,k)} = \mathcal{A}_c^{(i)}(\alpha_M^{(j,k)}) = \alpha_c^{(i,j,k)} - \left(J_m^{(i,j,k)} \right)^{-1} \mathcal{R}_m \left(\alpha_M^{(j,k)}, \alpha_c^{(i,j,k)} \right) \quad \text{with} \quad J_m^{(i,j,k)} := \frac{M_m}{\Delta t_k} + \frac{\partial \mathcal{F}_m^{(i,j,k)}}{\partial \alpha_c^{(i,j,k)}},$$

which yields immediately the derivative with respect to the macro scale

$$\frac{\partial \mathcal{A}_c^{(i)}}{\partial \alpha_M^{(j,k)}}(\alpha_M^{(j,k)}) \approx - \left(J_m^{(i,j,k)} \right)^{-1} \frac{\partial \mathcal{F}_m^{(i,j,k)}}{\partial \alpha_M^{(j,k)}}. \quad (4.4)$$

where the contribution from the Jacobian $J_m^{(i,j,k)}$ is disregarded due to Assumption (b). Summing up all contributions

$$\mathcal{A}_c(\alpha_M^{(j,k)}) = \sum_{i=1}^{N_{GP}} \mathcal{A}_c^{(i)}(\alpha_M^{(j,k)}),$$

plugging them into the macroscale stiffness matrix (3.9) and exploiting (4.4) concludes the proof

$$J_M^{(j,k)} = \frac{M_M}{\Delta t_k} + \frac{d\mathcal{F}_M}{d\alpha_M} \left(\alpha_M^{(j,k)}, \mathcal{A}_c(\alpha_M^{(j,k)}) \right) \stackrel{!}{=} \bar{J}_{\mathcal{F}}^{(j,k)}. \quad \square$$

In practice the assumptions (a) and (b) can be violated and one will end up with a different variant of the Newton–Raphson scheme. For example: the computation (4.4) involves the derivative of the correction terms \mathcal{A}_c with respect to the macroscale magnetic density α_M . In [3], it was proposed to solve several mesoscale problems per Gauß point in parallel: for a two-dimensional problem, $N_{dim}^m = 3$ problems were solved to approximate the Jacobian, the first one with the nominal macroscale source (e.g. $\alpha_M^{(i)}$) and the other two with a perturbed source magnetic density $\alpha_M^{(i)} + \delta^{(i)} \alpha_i$ where $\delta^{(i)}$ is a small perturbation and α_i is a vector oriented along the x , y or z -axes. Similarly, in 3D $N_{dim}^m = 4$ problems need to be solved. On the other hand, one can use a fixed point iteration scheme as suggested in [24], which is actually the limit case of a waveform relaxation approach, where time window size equals time step size.

Input: macroscale source \mathbf{j}_s and mesh.
Output: fields (macro/meso), global quantities.

```

1 begin
2    $t \leftarrow t_0$ , initialize the macroscale field  $\mathbf{a}_M|_{t_0} = \mathbf{a}_{M0}$ ,
3   # begin the macroscale time loop (index  $k$ )
4   for ( $k \leftarrow 1$  to  $N_{TS}$ ) do
5     # begin the macroscale NR loop (index  $j$ )
6     for ( $j \leftarrow 1$  to  $N_{NR}^M$ ) do
7       # parallel resolution of mesoscale problems (index  $i$ )
8       for ( $i \leftarrow 1$  to  $N_{GP}$ ) do
9         downscale the sources  $\boldsymbol{\alpha}_M^{(i,j,k-1)}$ ,
10        compute  $\boldsymbol{\alpha}_c^{(i,j,k)} = \mathcal{A}_c(\mathbf{y}, \boldsymbol{\alpha}_M^{(i,j,k)})$ , see Algorithm 2
11        compute the homogenized law  $\mathcal{H}_M^{(i,j,k)}$  and  $\partial \mathcal{H}_M^{(i,j,k)} / \partial \mathbf{b}_M^{(i,j,k)}$ ,
12        upscale the homogenized law  $\mathcal{H}_M^{(i,j,k)}$  and  $\partial \mathcal{H}_M^{(i,j,k)} / \partial \mathbf{b}_M^{(i,j,k)}$ ,
13      end
14      assemble the Jacobian  $J_M^{(j,k)} = \frac{1}{\Delta t_k} \mathbf{M}_M + \frac{d\mathcal{F}_M}{d\boldsymbol{\alpha}_M}(\boldsymbol{\alpha}_M^{(j,k)}, \mathcal{A}_c(\boldsymbol{\alpha}_M^{(j,k)}))$  to solve (3.12),
15    end
16  end
17 end

```

Algorithm 1: Pseudocode for the monolithic FE-HMM

Input: macroscale sources $\boldsymbol{\alpha}_M^{(i,j,k)}$ and the mesoscale mesh.
Output: homogenized law $\mathcal{H}_M^{(i,j,k)}$, per Gauß point for N_{dim}^m problems.

```

1 begin
2   prescribe periodic boundary conditions, impose sources,
3    $t \leftarrow t_M$ , initialize the correction  $\mathbf{a}_c|_{t_M}$ ,
4   solve  $N_{\text{dim}}^m$  mesoscale problems for the  $k^{\text{th}}$  time step,
5   for ( $p \leftarrow 1$  to  $N_{\text{dim}}^m$ ) do
6     # begin the mesoscale NR loop (index  $j$ )
7     for ( $j \leftarrow 1$  to  $N_{NR}^m$ ) do
8       assemble the Jacobian  $J_m^{(i,j,k)}$  to solve (3.13).
9     end
10  end
11 end

```

Algorithm 2: Pseudocode for one mesoscale problem

5. The waveform relaxation method

Waveform relaxation methods solve time dependent problems iteratively, i.e., they generalize the classical ideas of Gauß–Seidel and Jacobi iteration to the time domain. The method starts with an initial guess of the solution over a time interval and computes iteratively approximations of increasing accuracy [25]. Typically the problem is decomposed into subproblems and each subproblem is solved separately. Let us consider the two ordinary differential equations

$$\begin{aligned}\partial_t y_1 &= f_1(y_1, y_2) \\ \partial_t y_2 &= f_2(y_1, y_2).\end{aligned}$$

A monolithic or strongly coupled approach discretizes the problem in time as one system of equations. On the other hand, an iterative Gauß–Seidel type scheme

$$\begin{aligned}\partial_t y_1^{(l)} &= f_1(y_1^{(l)}, y_2^{(l-1)}) \\ \partial_t y_2^{(l)} &= f_2(y_1^{(l)}, y_2^{(l)})\end{aligned}$$

will resolve both equations subsequently, e.g., the first one for the unknown $y_1^{(l)}(t)$ on $t \in \mathcal{I}$ while considering $y_2^{(l-1)}(t)$ on $t \in \mathcal{I}$ given and vice-versa. The very first iteration requires an initial guess $y_2^{(0)}$, which is typically obtained by constant extrapolation, [26]. In the simplest case an implicit Euler method can be chosen for time stepping, e.g.

$$\begin{aligned}\frac{y_1^{(k,l)} - y_1^{(k-1,l)}}{\Delta t_k} &= f_1(y_1^{(k,l)}, y_2^{(k,l-1)}) \\ \frac{y_2^{(k,l)} - y_2^{(k-1,l)}}{\Delta t_k} &= f_2(y_1^{(k,l)}, y_2^{(k,l)})\end{aligned}$$

where $y_1^{(k,l)}$ describes the unknown y_1 at time t_k and iteration l ; Δt_k denotes the k -th time step size for both problems. Obviously, the iteration scheme allows to combine different time integrators with independent time step sizes. It is therefore often referred to as co-simulation or weak coupling. The convergence is well understood and unconditionally guaranteed for systems of ordinary differential equations [27, 28]. However, already in the case of simple differential algebraic equations, e.g. the system

$$\begin{aligned}\partial_t y_1^{(l)} &= f_1(y_1^{(l)}, z_1^{(l)}, y_2^{(l-1)}, z_2^{(l-1)}) \\ 0 &= g_1(y_1^{(l)}, z_1^{(l)}, y_2^{(l-1)}, z_2^{(l-1)}) \quad \text{with } \det \left(\frac{\partial g_1}{\partial z_1^{(l)}} \right) \neq 0 \\ \partial_t y_2^{(l)} &= f_2(y_1^{(l)}, z_1^{(l)}, y_2^{(l)}, z_2^{(l)}) \\ 0 &= g_2(y_1^{(l)}, z_1^{(l)}, y_2^{(l)}, z_2^{(l)}) \quad \text{with } \det \left(\frac{\partial g_2}{\partial z_2^{(l)}} \right) \neq 0\end{aligned}$$

the convergence of the fixed point iteration is conditional. In particular the dependence of algebraic equations on old algebraic iterates is critical, i.e., the Jacobian $\partial g_1 / \partial z_2^{(l)}$ must be sufficiently small, [29]. The convergence for more complex problems, possibly with higher DAE-index, is even more involved, [30].

Waveform relaxation has been originally applied in the simulation of electrical networks but has been applied in various disciplines. Recently, the method was rediscovered to cosimulate coupled problems [6]. The method converges particularly fast on small intervals and hence it is common to subdivide the time interval of interest into so called time windows and to apply the method on each time window separately. This subdivision does not hinder the overall convergence since the error propagation from windows to window can be controlled [31]. Waveform relaxation is a particular parallel-in-time methods and hence closely linked to Parareal [32, 33] which has also recently been applied to multiscale problems [34].

6. Waveform Relaxation HMM

We employ a waveform relaxation-based approach with windowing [5]. Weak forms similar to (3.1) for the macroscale and (3.6) for the mesoscale problem are solved on a series of time windows $\mathcal{I}_n = (t_{n-1}, t_n] \subset \mathcal{I}$ ($n = 1, 2, \dots, N_{\text{TW}}$). On each time window, macroscale and mesoscale problems are solved separately in time-domain, such that waveforms, e.g., $\boldsymbol{\alpha}_M(t)$, are obtained. Afterwards the coupling between the problems is introduced by exchanging the waveforms, and solving the system iteratively. In each waveform relaxation iteration l , the resolution of mesoscale problems (for instance with solutions $\boldsymbol{\alpha}_c^{(l)}(t)$), is followed by the resolution of the macroscale problem (for instance with the solution $\boldsymbol{\alpha}_M^{(l)}(t)$) until convergence is reached (for instance $\|\boldsymbol{\alpha}_M^{(l-1)} - \boldsymbol{\alpha}_M^{(l)}\|_{L^\infty(0, T; L^2(\Omega))} < \text{tol}_M$). In the rest of the section, we will often omit the time window index n to simplify notation (for instance $\boldsymbol{\alpha}_M^{(j, k, l, n)}$ and $\boldsymbol{\alpha}_c^{(i, j, k, l, n)}$ become $\boldsymbol{\alpha}_M^{(j, k, l)}$ and $\boldsymbol{\alpha}_c^{(i, j, k, l)}$, respectively).

For any given waveform relaxation iteration l , N_{GP} mesoscale problems are solved (in parallel) using the macroscale source terms from the previous waveform iteration $l-1$. In the following section we discuss these two problems starting with the macroscale.

6.1. The macroscale problem

The waveform relaxation starts with the resolution of mesoscale problems. The solutions $\boldsymbol{\alpha}_c^{(i, k, l, n)}$ are then used for computing the homogenized constitutive law needed by the nonlinear macroscale problem derived from the semi-discrete equations (3.12):

$$\mathbf{M}_M \frac{\boldsymbol{\alpha}_M^{(k, l)} - \boldsymbol{\alpha}_M^{(k-1, l)}}{\Delta t_k} + \mathcal{F}_M \left(\boldsymbol{\alpha}_M^{(k, l)}, \boldsymbol{\alpha}_c^{(k, l)} \right) = 0 \quad (6.1)$$

with known (mesoscale) corrections $\boldsymbol{\alpha}_c^{(k, l)}$ at time points t_k . The macroscale and the mesoscale problems are decoupled and the homogenized constitutive law $\mathcal{H}_M^{(k, l)}$ used in (6.1) is upscaled using the formula

$$\mathcal{H}_M^{(k, l)}(\mathbf{x}, t, \mathbf{b}_M(\mathbf{x}, t)) = \frac{1}{|\Omega_m|} \int_{\Omega_m} \mathcal{H}(\mathbf{x}, \mathbf{y}, \mathbf{b}_c^{(k, l)}(\mathbf{x}, \mathbf{y}, t) + \mathbf{b}_M(\mathbf{x}, t)) d\mathbf{y}.$$

with $\mathbf{b}_M = \text{curl}_x \mathbf{a}_M$ and where the mesoscale field $\mathbf{b}_c^{(k, l)} = \text{curl}_y \mathbf{a}_c^{(k, l)}$ is obtained by solving mesoscale problems for a waveform relaxation iteration l as explained in Section 6.2. The decoupling between the macroscale and the mesoscale problems allows to compute the homogenized Jacobian directly by

$$\frac{\partial \mathcal{H}_M^{(k, l)}}{\partial \boldsymbol{\alpha}_M} = \frac{1}{|\Omega_m|} \int_{\Omega_m} \left(\frac{\partial \mathcal{H}}{\partial \mathbf{b}_M}(\mathbf{b}_c^{(k, l)} + \mathbf{b}_M) \frac{\partial \mathbf{b}_M}{\partial \boldsymbol{\alpha}_M} \right) d\mathbf{y}, \quad (6.2)$$

since \mathcal{H} is known as a closed-form expression. This results from the independence of the mesoscale solutions $\boldsymbol{\alpha}_c^{(k, l)}$ on the macroscale source $\boldsymbol{\alpha}_M^{(k, l)}$. Indeed, each mesoscale problem corresponding to the Gauß point denoted by i is computed using the macroscale fields from the previous waveform relaxation iteration

$$\boldsymbol{\alpha}_c^{(k, l)} = \mathcal{A}_c(\boldsymbol{\alpha}_M^{(k, l-1)}).$$

Unlike the mesoscale problem in (3.4) which was strongly coupled with the macroscale problem, the function \mathcal{A}_c is evaluated at each $\boldsymbol{\alpha}_M^{(i, k, l-1)}$ and there is no need to evaluate the derivative $\partial \mathcal{A}_c / \partial \boldsymbol{\alpha}_M$ using the finite difference method as done in (4.4). Note however that one mesoscale field computation per Gauß point is needed for each waveform relaxation iteration.

Let us consider the case of a quasi-linear law as e.g. Brauer's model [10]:

$$\mathcal{H}(\mathbf{b}) = \mu(\mathbf{b}) \mathbf{b}$$

with $\mathbf{b} = \mathbf{b}_M + \mathbf{b}_c^{(k, l)}$, the integrand in (6.1) is calculated using

$$\frac{\partial \mathcal{H}(\mathbf{b})}{\partial \mathbf{b}_M} = \mu(\mathbf{b}) + \frac{\partial \mu}{\partial |\mathbf{b}|^2} \frac{\partial |\mathbf{b}|^2}{\partial \mathbf{b}_M} \otimes \mathbf{b} = \mu(\mathbf{b}) + 2 \frac{\partial \mu}{\partial |\mathbf{b}|^2} \mathbf{b} \otimes \mathbf{b}$$

where \otimes denotes the square dyadic product.

6.2. Mesoscale problems

Starting from the mesoscale semi-discrete equations (3.13) of Problem 3.4, the following nonlinear mesoscale problems are derived for the l^{th} waveform iteration:

$$\mathbf{M}_m \frac{\boldsymbol{\alpha}_c^{(i,k,l)} - \boldsymbol{\alpha}_c^{(i,k-1,l)}}{\Delta t_k} + \mathcal{F}_m \left(\boldsymbol{\alpha}_c^{(i,k,l)}, \boldsymbol{\alpha}_M^{(k,l-1)} \right) = 0, \quad i = 1, \dots, N_{\text{GP}}. \quad (6.3)$$

with known (macroscale) waveforms $\boldsymbol{\alpha}_M^{(k,l-1)}$ (given at time points t_k). In this equation, the macroscale source per Gauß point $\boldsymbol{\alpha}_M^{(i,l-1)}$ is considered to be known and taken from the previous waveform relaxation iteration $l-1$. The mesoscale problems defined in (6.3) can then be solved in parallel on the time window \mathcal{I}_n and the mesoscale solutions stored for all Gauß points of the macroscale grid. These solutions are later used for computing the homogenized material law and the Jacobian as described in Section 6.1. The mesoscale corrections \mathbf{b}_c appearing in (6.1) is independent from the macroscale field \mathbf{b}_M .

If an implicit Euler scheme is used for the macroscale and the mesoscale problems, the overall discretized system consists in solving the following problem:

Problem 6.1 (Nonlinear, discrete, WR multiscale problem). *Find a series of solutions*

$$[\boldsymbol{\alpha}_M^{(k,l)}, \boldsymbol{\alpha}_c^{(1,k,l)}, \dots, \boldsymbol{\alpha}_c^{(N_{\text{GP}},k,l)}] \in \mathbb{R}^{N_M + N_{\text{GP}} \cdot N_c}$$

such that

$$\mathcal{R}_M \left(\boldsymbol{\alpha}_M^{(k,l)}, \boldsymbol{\alpha}_c^{(i,k,l)} \right) = \mathbf{M}_M \frac{\boldsymbol{\alpha}_M^{(k,l)} - \boldsymbol{\alpha}_M^{(k-1,l)}}{\Delta t_k} + \mathcal{F}_M \left(\boldsymbol{\alpha}_M^{(k,l)}, \boldsymbol{\alpha}_c^{(i,k,l)} \right) = 0$$

and for the mesoscale problems $i = 1, \dots, N_{\text{GP}}$

$$\mathcal{R}_m \left(\boldsymbol{\alpha}_M^{(k,l-1)}, \boldsymbol{\alpha}_c^{(i,k,l)} \right) = \mathbf{M}_m \frac{\boldsymbol{\alpha}_c^{(i,k,l)} - \boldsymbol{\alpha}_c^{(i,k-1,l)}}{\Delta t_k} + \mathcal{F}_m \left(\boldsymbol{\alpha}_c^{(i,k,l)}, \boldsymbol{\alpha}_M^{(k,l-1)} \right) = 0.$$

Let $\boldsymbol{\alpha}_M^{(j,k,l)}$ and $\boldsymbol{\alpha}_c^{(i,j,k,l)}$ denote the j^{th} Newton–Raphson iterates. Then we define

$$\mathcal{F}_M^{(j,k,l)} := \mathcal{F}_M \left(\boldsymbol{\alpha}_M^{(j,k,l)}, \boldsymbol{\alpha}_c^{(i,j,k,l)} \right), \quad \mathcal{F}_m^{(i,j,k,l)} := \mathcal{F}_m \left(\boldsymbol{\alpha}_c^{(i,j,k,l)}, \boldsymbol{\alpha}_M^{(j,k,l)}, \frac{\boldsymbol{\alpha}_M^{(i,j,k,l)} - \boldsymbol{\alpha}_M^{(i,j,k-1,l)}}{\Delta t_k} \right). \quad (6.4)$$

The following total Jacobian must be computed to resolve Problem 6.1:

$$\mathbf{J}_{\mathcal{R}}^{(j,k,l)} = \frac{1}{\Delta t_k} \begin{pmatrix} \mathbf{M}_M & 0 & \cdots & 0 \\ 0 & \mathbf{M}_m & 0 & 0 \\ \vdots & 0 & \ddots & 0 \\ 0 & 0 & 0 & \mathbf{M}_m \end{pmatrix} + \begin{pmatrix} \frac{\partial \mathcal{F}_M^{(j,k,l)}}{\partial \boldsymbol{\alpha}_M^{(j,k,l)}} & \frac{\partial \mathcal{F}_M^{(j,k,l)}}{\partial \boldsymbol{\alpha}_c^{(1,j,k,l)}} & \cdots & \frac{\partial \mathcal{F}_M^{(j,k,l)}}{\partial \boldsymbol{\alpha}_c^{(N_{\text{GP}},j,k,l)}} \\ 0 & \frac{\partial \mathcal{F}_m^{(1,j,k,l)}}{\partial \boldsymbol{\alpha}_c^{(1,j,k,l)}} & 0 & 0 \\ \vdots & 0 & \ddots & 0 \\ 0 & 0 & 0 & \frac{\partial \mathcal{F}_m^{(N_{\text{GP}},j,k,l)}}{\partial \boldsymbol{\alpha}_c^{(N_{\text{GP}},j,k,l)}} \end{pmatrix}. \quad (6.5)$$

The decoupling of mesoscale from the macroscale solution makes all the elements of the first column equal to zero except for $\partial \mathcal{F}_M^{(j,k,l)} / \partial \boldsymbol{\alpha}_M^{(j,k,l)}$. Let us state the following result for the sake of completeness:

Proposition 6.1. *The use of the Jacobian (6.5) for solving the waveform relaxation problem is equivalent to the resolution of the following decoupled system for each waveform relaxation iteration l :*

$$\bar{\mathbf{J}}_{\mathcal{F}}^{(j,k,l)} = \frac{\mathbf{M}_M}{\Delta t_k} + \frac{\partial \mathcal{F}_M^{(j,k,l)}}{\partial \boldsymbol{\alpha}_M^{(j,k,l)}}$$

Input: macroscale source \mathbf{j}_s and mesh.

Output: fields (macro/meso), global quantities.

```

1 begin
2   # begin loops over time windows (index n)
3   for (n ← 1 to NTW) do
4     # begin waveform relaxation (WR) loop (index l)
5     for (l ← 1 to NWR) do
6       # 1. Parallel resolution of meso-problems (index i)
7       for (i ← 1 to NGP) do
8         | downscale the sources  $\alpha_M^{(l-1)}$ ,
9         | solve mesoscale problems (1 per Gauß point) on  $[t_k, t_{k+1}]$ ,
10        | save the solution,
11        end
12        # 2. Resolution of the macro-problem on  $[t_k, t_{k+1}]$ 
13         $t \leftarrow t_k$ , initialize the macro-field  $\mathbf{a}_M|_{t_k} = \mathbf{a}_{Mk}$ ,
14        # begin the macroscale time loop(index k)
15        for (k ← 1 to NTS) do
16          # begin the macroscale NR loop (index j)
17          for (j ← 1 to NNRM) do
18            # parallel updating of the homogenized law (index i)
19            for (i ← 1 to NGP) do
20              | Read the mesoscale fields  $\mathbf{b}_m^{(l)}$ ,
21              | update  $\partial\mathcal{H}_M^{(l)}/\partial\mathbf{b}_M^{(l)}$  using (6.1),
22              | upscale the law  $\mathcal{H}_M^{(l)}, \partial\mathcal{H}_M^{(l)}/\partial\mathbf{b}_M^{(l)}$ ,
23            end
24            assemble the matrix and solve,
25          end
26        end
27      end
28    end
29 end

```

Algorithm 3: Pseudocode for the waveform relaxation FE-HMM.

Proof. The application of the Schur complement to (6.5) leads to the conclusion. \square

The implementation of the waveform relaxation method is illustrated in Algorithm 3. We propose a Gauß–Seidel type scheme between the macro- and the mesoscale, where the mesoscale is solved in parallel. It starts with a loop over time windows and for each time window, a waveform relaxation loop involving weakly coupled macroscale and mesoscale problems is carried out. The mesoscale are solved in parallel on the time interval \mathcal{I}_n using the macroscale sources from the previous WR iteration $\mathbf{a}_M^{(l-1)}$ in the mesoscale problems. Mesoscale solutions are then stored for later use in the evaluation of the homogenized magnetic field and of the Jacobian. Then the macroscale problem is solved on \mathcal{I}_n until convergence. The resolution involves a time discretization that leads to a nonlinear problem that is solved using the Newton–Raphson method with the Jacobian evaluated using the previously stored mesoscale fields.

Ultimately, the solution of the entire multiscale problem is obtained as follows (only superscripts of the waveform relaxation and the time window are involved, i.e., the fields involved are $\mathbf{a}_c^{(l,n)}$ and $\mathbf{a}_M^{(l,n)}$): the macroscale field $\mathbf{a}_M^{(0,n)}$ is initialized with constant extrapolation. The mesoscale problem can then be solved for the first iteration, i.e., one obtains $\mathbf{a}_c^{(1,n)}$. This is then used for successive waveform relaxation iterations

$$\begin{array}{cccccccc}
 \mathbf{a}_M^{(0,1)} & \rightarrow & \mathbf{a}_c^{(1,1)} & \rightarrow & \mathbf{a}_M^{(1,1)} & \rightarrow & \mathbf{a}_c^{(2,1)} & \rightarrow \dots \rightarrow \mathbf{a}_M^{(N_{\text{WR}},1)} \\
 \mathbf{a}_M^{(0,2)} & \rightarrow & \mathbf{a}_c^{(1,2)} & \rightarrow & \mathbf{a}_M^{(1,2)} & \rightarrow & \mathbf{a}_c^{(2,2)} & \rightarrow \dots \rightarrow \mathbf{a}_M^{(N_{\text{WR}},2)}, \\
 & & & & \vdots & & & \\
 \mathbf{a}_M^{(0,N_{\text{TW}})} & \rightarrow & \mathbf{a}_c^{(1,N_{\text{TW}})} & \rightarrow & \mathbf{a}_M^{(1,N_{\text{TW}})} & \rightarrow & \mathbf{a}_c^{(2,N_{\text{TW}})} & \rightarrow \dots \rightarrow \mathbf{a}_M^{(N_{\text{WR}},N_{\text{TW}})}.
 \end{array}$$

In addition to the flexible use of different FE bases and meshes at both scales, this approach also provides a natural setting for the use of different integrators and time step sizes. Communication costs can also be reduced in the case of parallel computations. As a drawback, the number of iterations for solving both the macroscale and the mesoscale problems may increase. A rigorous convergence analysis requires a structural analysis of the coupled problem (3.10)–(3.11). In particular, the DAE index [35] must be known to guarantee convergence, c.f. [30]. This analysis is beyond the scope of this paper. However, the total costs for the monolithic and the waveform relaxation methods are estimated in the next Section.

7. Estimation of the computational cost

In this section, we evaluate and compare total computational costs of the monolithic and the waveform relaxation algorithms. The total cost comprises the computational and the communication costs, which differ from one algorithm to the other. We use $C_{\text{sol}}^m, C_{\text{com}}, C_{\text{ass}}^M$ and C_{sol}^M for the one time step costs for the mesoscale computations (including Newton iterations), the mesoscale–macroscale communications, the macroscale assembling and the macroscale resolution, respectively. C_{sol}^m is the most expensive and dominant operation. The total number of time steps is denoted by N_{TS} and the number of time windows N_{TW} , such that the computational costs for a time window with $N_{\text{TS}}/N_{\text{TW}}$ time steps are roughly $\frac{N_{\text{TS}}}{N_{\text{TW}}} C_{\text{sol}}^m$.

7.1. Monolithic HMM

The total cost of the monolithic algorithm is given by

$$C_{\text{Mono}} = C_{\text{Mono}}^m + C_{\text{Mono}}^M, \quad (7.1)$$

and has two contributions: the mesoscale contribution

$$C_{\text{Mono}}^m = N_{\text{TS}} N_{\text{NR}}^M N_{\text{GP}} (N_{\text{dim}}^m C_{\text{sol}}^m + C_{\text{com}}), \quad (7.2)$$

and the macroscale contribution

$$C_{\text{Mono}}^M = N_{\text{TS}} N_{\text{NR}}^M (C_{\text{ass}}^M + C_{\text{sol}}^M), \quad (7.3)$$

where N_{TS} is the total number of time steps, N_{NR}^{M} and N_{NR}^{m} are the average numbers of Newton–Raphson iterations for macroscale and mesoscale problems to converge, $N_{\text{dim}}^{\text{m}}$ is the number of problems solved to approximate the Jacobian and the other N_{\star} are defined in Table 1.

The total cost in (7.1) can be understood from the Algorithms 1 and 2. The overall problem is discretized in N_{TS} macroscale time steps and a macroscale nonlinear system is solved for each time step using the Newton–Raphson scheme. Therefore, N_{NR}^{M} nonlinear (Newton–Raphson) iterations are performed for each time step. Each of these iterations involves the evaluation of the Jacobian at N_{GP} Gauß points by solving $N_{\text{dim}}^{\text{m}} = 3$ or 4 mesoscale problems. The macroscale linear system is then assembled and solved. The mesoscale cost $C_{\text{sol}}^{\text{m}}$ involves the resolution of nonlinear mesoscale problems over one time step. N_{NR}^{m} nonlinear iterations are needed for each time step at the mesoscale and $2N_{\text{TS}}N_{\text{NR}}^{\text{M}}N_{\text{GP}}$ communications involving the parallel transfer of small chunks of information are needed for the overall time interval. The macroscale assembling and resolution costs can be disregarded with respect to the mesoscale costs, therefore

$$C_{\text{Mono}} \approx C_{\text{Mono}}^{\text{m}}.$$

7.2. Waveform relaxation HMM

The total cost for the WR algorithm is given by:

$$C_{\text{WR}} = C_{\text{WR}}^{\text{m}} + C_{\text{WR}}^{\text{M}}. \quad (7.4)$$

In the general case where N_{TW} time windows $\mathcal{I}_n = (t_n, t_{n+1}]$ are used. The two contributions in (7.4) are the mesoscale cost

$$C_{\text{WR}}^{\text{m}} = N_{\text{TS}} N_{\text{WR}} N_{\text{GP}} \left(C_{\text{sol}}^{\text{m}} + \frac{N_{\text{TW}}}{N_{\text{TS}}} C_{\text{com}} \right) \quad (7.5)$$

$$= N_{\text{TS}} N_{\text{WR}} N_{\text{GP}} C_{\text{sol}}^{\text{m}} + N_{\text{TW}} N_{\text{WR}} N_{\text{GP}} C_{\text{com}}, \quad (7.6)$$

and the macroscale cost

$$C_{\text{WR}}^{\text{M}} = N_{\text{TW}} N_{\text{WR}} N_{\text{NR}}^{\text{M}} (N_{\text{GP}} C_{\text{jac}}^{\text{m}} + C_{\text{ass}}^{\text{M}} + C_{\text{sol}}^{\text{M}}). \quad (7.7)$$

Additionally, $C_{\text{jac}}^{\text{m}}$ is the cost for reading a pre-stored mesoscale field map and evaluating the Jacobian for all time steps of the time window using (6.1) for each time step, and N_{NR}^{M} is the average number of Newton–Raphson iterations for macroscale problems to converge. These costs can be made small compared to the mesoscale computational cost $C_{\text{dim}}^{\text{m}}$ and the communication cost C_{com} by the use of a smart implementation.

The total cost in (7.4) can be understood from the Algorithm 3. The overall problem is discretized and solved on N_{TW} time windows and for each time window \mathcal{I}_n , a waveform relaxation loop involving N_{WR} WR iterations during which mesoscale problems are solved and stored. The communication cost involves the transfer of $\frac{N_{\text{TS}}}{N_{\text{TW}}} N_{\text{GP}} N_{\text{NR}}$ communications of bigger chunks of informations for each time window.

The nonlinear macroscale problem is solved using the Newton–Raphson scheme. Therefore, N_{NR}^{M} nonlinear iterations are carried for each time step and for each Newton–Raphson iteration, the Jacobian is computed for N_{GP} Gauß points. This is done by reading mesoscale field maps for each Gauß point and then evaluating the homogenized law using (6.1). The macroscale linear system is then assembled and solved. The reading of mesoscale fields maps and the update of the homogenized law are one of the leverage for accelerating computations in the context of the waveform relaxation method.

Neglecting the macroscale assembling and resolution costs, equation (7.4) can be approximated by

$$C_{\text{WR}} \approx N_{\text{TS}} N_{\text{WR}} N_{\text{GP}} \left(C_{\text{sol}}^{\text{m}} + \frac{N_{\text{TW}}}{N_{\text{TS}}} (N_{\text{NR}}^{\text{M}} C_{\text{jac}}^{\text{m}} + C_{\text{com}}) \right),$$

where N_{TS} is the total number of time steps. The following theorem allows to compare computational costs for the monolithic and the waveform relaxation approaches.

Theorem 7.1. *The computational costs for the monolithic and the waveform relaxation methods are respectively given by the following approximations:*

$$C_{\text{Mono}} \approx N_{\text{TS}} N_{\text{NR}}^{\text{M}} N_{\text{GP}} (N_{\text{dim}}^{\text{m}} C_{\text{sol}}^{\text{m}} + C_{\text{com}}), \quad (7.8)$$

and

$$C_{\text{WR}} \approx N_{\text{TS}} N_{\text{WR}} N_{\text{GP}} \left(C_{\text{sol}}^{\text{m}} + \frac{N_{\text{TW}}}{N_{\text{TS}}} (N_{\text{NR}}^{\text{M}} C_{\text{jac}}^{\text{m}} + C_{\text{com}}) \right). \quad (7.9)$$

Proof. The theorem results from the developments of Sections 7.1 and 7.2. The high level of parallelization as explained in Algorithms 1-2 and 3 results from the independence of mesoscale problems. \square

Moreover, the two approaches can easily be parallelized.

Remark 7.2. *The computational cost of the waveform relaxation method can be decreased by minimizing the cost related to the reading of the mesoscale fields and the update of the homogenized law.*

Assume that there exists $\kappa \in (0, 1)$ such that

$$\frac{N_{\text{TW}}}{N_{\text{TS}}} N_{\text{NR}}^{\text{M}} C_{\text{jac}}^{\text{m}} = \kappa (C_{\text{sol}}^{\text{m}} + \frac{N_{\text{TW}}}{N_{\text{TS}}} C_{\text{com}})$$

which is a reasonable assumption because the cost due to the computation of the material law using the pre-stored mesoscale maps on the whole time window is small compared to the cost due to the computation of mesoscale problems on the same time window and the communication. Then the relationship

$$\begin{aligned} N_{\text{WR}} \left(C_{\text{sol}}^{\text{m}} + \frac{N_{\text{TW}}}{N_{\text{TS}}} (N_{\text{NR}}^{\text{M}} C_{\text{jac}}^{\text{m}} + C_{\text{com}}) \right) &= N_{\text{WR}} \left((1 + \kappa) C_{\text{sol}}^{\text{m}} + \frac{N_{\text{TW}}}{N_{\text{TS}}} (1 + \kappa) C_{\text{com}} \right) \\ &< N_{\text{NR}}^{\text{M}} (N_{\text{dim}}^{\text{m}} C_{\text{sol}}^{\text{m}} + C_{\text{com}}) \end{aligned}$$

between (7.8) and (7.9) shows that the waveform relaxation method is more efficient if

$$N_{\text{WR}} < \frac{N_{\text{dim}}^{\text{m}}}{(1 + \kappa)} N_{\text{NR}}^{\text{M}} \quad (7.10)$$

and each time window consists of at least $N_{\text{TS}} > 2$ time steps which is a rather technical assumption. As can be seen from relation (7.10), reducing the number of time windows (N_{TW}) reduces the communication cost between the mesoscale and macroscale problems. Additionally, the reduction of cost due to the evaluation of the Jacobian minimizes the overall cost of the waveform relaxation method.

8. Application

We use a soft magnetic composite (SMC) material to test the ideas developed in the previous sections. An idealized 2D periodic SMC (with 20×20 grains) surrounded by an inductor is considered.

For the first series of numerical tests we use the SMC structure depicted in Figure 3 (only 10×10 grains are shown). The geometry has been chosen such that the vector potential formulation $\mathbf{b} = \text{curl } \mathbf{a}$ as described in Section 2 with $\mathbf{a} = (0, 0, a_z)$ can be used. The magnetic flux density $\mathbf{b} = (b_x, b_y, 0)$ lives in the xy -plane. Only a quarter of the structure is considered for numerical computations thanks to the symmetry (see Figure 4 - left for the reference geometry and Figure 4 - right for the geometry used for the homogenized problem). In both cases, the following boundary conditions are imposed on $\Gamma_{\text{inf}}, \Gamma_{\text{h}}$ and Γ_{v} :

$$(\mathbf{n} \cdot \mathbf{b})|_{\Gamma_{\text{inf}}} = 0 \Leftrightarrow (\mathbf{n} \times \mathbf{a})|_{\Gamma_{\text{inf}}} = \mathbf{0}, \quad (\mathbf{n} \cdot \mathbf{b})|_{\Gamma_{\text{h}}} = 0 \Leftrightarrow (\mathbf{n} \times \mathbf{a})|_{\Gamma_{\text{h}}} = \mathbf{0}, \quad (\mathbf{n} \times \mathbf{h})|_{\Gamma_{\text{v}}} = \mathbf{0}.$$

Using Ampère's equation (2.2 a), the source current \mathbf{j}_{s} must be imposed perpendicular to the xy -plane $\mathbf{j}_{\text{s}} = (0, 0, j_s)$ with $j_s = j_{s0} s(t) = j_{s0} \sin(2\pi f t)$. We consider the operating frequency $f = 50$ kHz which corresponds to $\lambda = 6000\text{m}$. The wavelength of the source is much larger compared to the length of the structure ($\simeq 500\mu\text{m}$) so that the assumption of a magnetoquasistatic problem can be made.

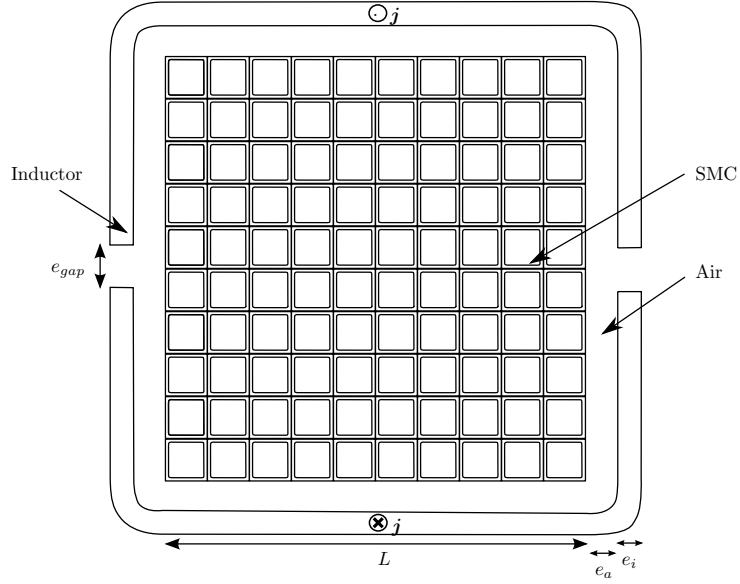


Figure 3: Soft magnetic composite two-dimensional used geometry. Two opposite source current are imposed in the top and bottom inductors. The lengths are given by $L = 1000 \mu\text{m}$, $e_a = 150 \sqrt{2}/2 \mu\text{m}$, $e_i = 100 \mu\text{m}$ and $e_{gap} = 100 \mu\text{m}$. Only 100 grains out of 400 are drawn on the image.

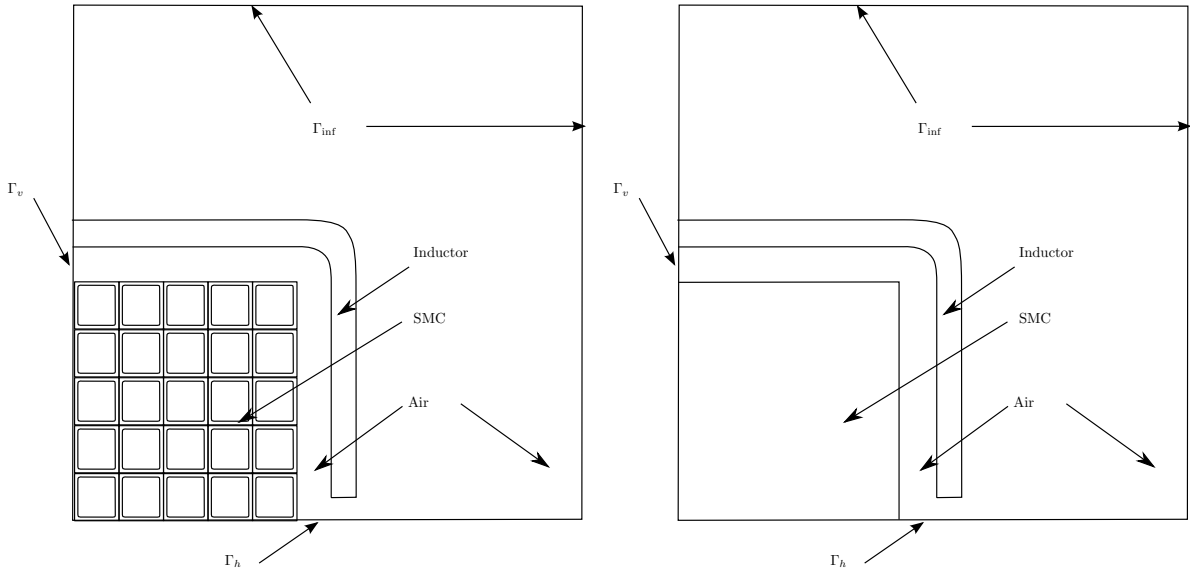


Figure 4: Geometry used for computations. Only a quarter of the geometry is used thanks to the symmetries. Left: reference geometry. Only 25 grains out of 100 are drawn on the image. Right: homogenized geometry.

We consider isotropic materials and therefore, the magnetic field \mathbf{h} has only xy components. We use the same material properties as those used in [2]: the insulation material is linear isotropic (with $\mu_r = 1$ and $\sigma = 0$). The conductor has an isotropic electric conductivity $\sigma = 5 \text{ MS}$ and is also governed by the following nonlinear magnetic law [10]:

$$\mathcal{H}(\mathbf{b}^\varepsilon) = \left(\alpha + \beta \exp(\gamma \|\mathbf{b}^\varepsilon\|^2) \right) \mathbf{b}^\varepsilon$$

with $\alpha = 388$, $\beta = 0.3774$ and $\gamma = 2.97$. The reference solution is obtained by solving a FE problem on an extremely fine mesh (347,324 elements) of the whole SMC structure. The mesoscale problems are solved on a square elementary cell meshed with (4,215 elements). Results obtained using the newly developed waveform relaxation (WR) approach subscripted WR are compared to the reference results (subscripted “Ref”) obtained solving the reference problem (2.6) on a very fine mesh and results of the monolithic approach (subscripted “Mono”) obtained solving problem (3.1) and (3.6).

Quantities of interest (global quantities and errors) are defined and used for numerical validation. The global quantities are the reference, the monolithic and the WR eddy currents losses:

$$\tau P_{\text{Ref}}(t) = q(\mathbf{a}^\varepsilon), \quad \tau P_{\text{mono}}(t) = q(\mathbf{a}_m), \quad \tau P_{\text{WR}}^l(t) = q(\mathbf{a}_m^l),$$

where the functionals q is defined as:

$$q(\mathbf{u}) = \begin{cases} \int_{\Omega_\varepsilon} (\sigma |\partial_t \mathbf{u}^\varepsilon(\mathbf{x}, t)|) dx & \text{if } \mathbf{u} \text{ is the reference solution} \\ \int_{\Omega} \left(\frac{1}{|\Omega_m|} \int_{\Omega_{mc}} (\sigma |\partial_t \mathbf{u}_m(\mathbf{x}, \mathbf{y}, t)|^2) dy \right) dx & \text{if } \mathbf{u} \text{ is the solution of the multiscale method} \end{cases}$$

Equivalent quantities can be defined in terms of the magnetic energy and the magnetic power. Two types of errors are defined: the relative error on global quantities

$$\text{Err}_{\tau P}^l = \delta_{\text{rel}}(\tau P_{\text{WR}}^l, \tau P_{\text{Mono}}), \quad \text{Err}_{\text{Wmag}}^l = \delta_{\text{rel}}(\text{Wmag}_{\text{WR}}^l, \text{Wmag}_{\text{Mono}}), \quad (8.1)$$

and the relative error on the fields \mathbf{u}_M

$$\text{Err}_{\mathbf{u}}^{(l)} = \bar{\delta}_{\text{rel}}(\mathbf{u}_M) \quad (8.2)$$

where \mathbf{u} stand for the fields \mathbf{b}_M , $\partial_t \mathbf{a}_M$ and $\partial_t \mathbf{b}_M$. The functions δ_{rel} and $\bar{\delta}_{\text{rel}}$ are defined by:

$$\delta_{\text{rel}}(v, w) = \frac{\|v - w\|_{L^\infty(0, T)}}{\|w\|_{L^\infty(0, T)}}, \quad \bar{\delta}_{\text{rel}}(\mathbf{u}) = \frac{\|\mathbf{u}^l - \mathbf{u}^{l-1}\|_{L^\infty(0, T; \mathbf{L}^\infty(\Omega))}}{\|\mathbf{u}^0\|_{L^\infty(0, T; \mathbf{L}^\infty(\Omega))}}.$$

8.1. Numerical convergence analysis

The monolithic HMM and the WR HMM algorithms have been implemented in the open source software GetDP [36] using a finite element formulation. Two cases are considered for the numerical validation of the method: (a) the case with 1 time window and the same time stepping at the macroscale and the mesoscale; (b) the case with 1 time window and different time stepping at the macroscale and the mesoscale.

For case (a), an excellent agreement is obtained between the WR solutions and the monolithic solutions to which the monolithic solutions are expected to converge for the eddy current losses (Figure 5 - left) and the magnetic energy (Figure 5 - right). Table 2 depicts the evolution of the relative L^∞ error defined in (8.1) on eddy currents losses and the magnetic energy between the WR and the monolithic approach. As can be seen from this table, the error between the WR and the monolithic cases is smaller than the error between the monolithic and the reference cases after the third WR iteration. These findings were verified for all the numerical tests that were run. Figure 6 - left. Left depicts the evolution of the relative L^∞ error on the electromagnetic fields defined in (8.2) as a function of the WR iterations. This criterion is to be used to control the error in case the monolithic solution is not available.

Also for case (b) a good agreement is obtained between the waveform relaxation solutions and the monolithic solutions. Figure 6 - right illustrates the case with different macroscale time discretization (10, 25 and 50 time steps per period) but with the same time discretization at the mesoscale (50 time steps per period). In particular, a good agreement is observed for values of the error up to 10^{-4} . Beyond this

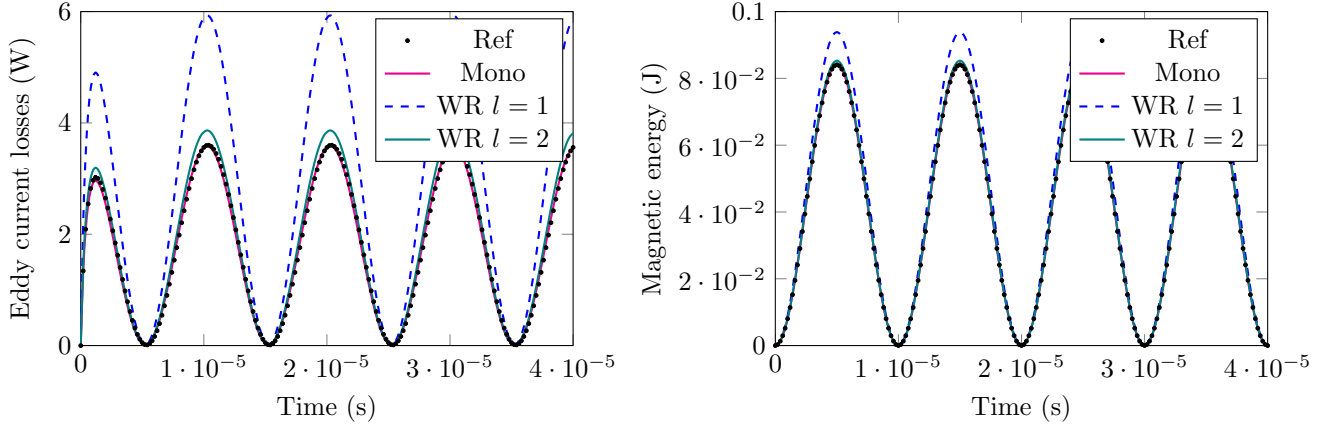


Figure 5: Instantaneous eddy current losses (left) and magnetic power (right) for the reference, the monolithic and the WR approaches. An overall mesh of 8722 elements with 25 elements for the homogenized domain and a time step $\Delta t = 2 \cdot 10^{-7}$ s were used. Only results for the first two WR iterations are shown.

Table 2: Convergence of the eddy current losses and the magnetic energy as a function of the WR iterations. The relative errors $\text{Err}_{\tau P}$ and $\text{Err}_{W_{\text{mag}}}$ between the reference and the monolithic approaches are $2.12 \cdot 10^{-2}$ and $1.24 \cdot 10^{-2}$, respectively.

WR iteration l	$\text{Err}_{\tau P}^l$	$\text{Err}_{\tau P}^l - \text{Err}_{\tau P}^{l-1}$	$\text{Err}_{W_{\text{mag}}}^l$	$\text{Err}_{W_{\text{mag}}}^l - \text{Err}_{W_{\text{mag}}}^{l-1}$
1	$6.68 \cdot 10^{-1}$	—	$1.17 \cdot 10^{-1}$	—
2	$8.08 \cdot 10^{-2}$	$5.87 \cdot 10^{-1}$	$1.45 \cdot 10^{-2}$	$1.03 \cdot 10^{-1}$
3	$1.17 \cdot 10^{-2}$	$6.90 \cdot 10^{-2}$	$2.08 \cdot 10^{-3}$	$1.24 \cdot 10^{-2}$
4	$1.87 \cdot 10^{-3}$	$9.84 \cdot 10^{-3}$	$3.18 \cdot 10^{-4}$	$1.77 \cdot 10^{-3}$
5	$3.78 \cdot 10^{-4}$	$1.49 \cdot 10^{-3}$	$5.01 \cdot 10^{-5}$	$2.68 \cdot 10^{-4}$
6	$1.41 \cdot 10^{-4}$	$2.35 \cdot 10^{-4}$	$8.00 \cdot 10^{-6}$	$4.21 \cdot 10^{-5}$
7	$1.05 \cdot 10^{-4}$	$3.80 \cdot 10^{-5}$	$1.30 \cdot 10^{-6}$	$6.70 \cdot 10^{-6}$
8	$9.0 \cdot 10^{-5}$	$6.00 \cdot 10^{-6}$	$2.00 \cdot 10^{-6}$	$1.10 \cdot 10^{-6}$
9	$9.8 \cdot 10^{-5}$	$< 10^{-6}$	$< 10^{-6}$	$< 10^{-6}$
10	$9.8 \cdot 10^{-5}$	$< 10^{-6}$	$< 10^{-6}$	$< 10^{-7}$

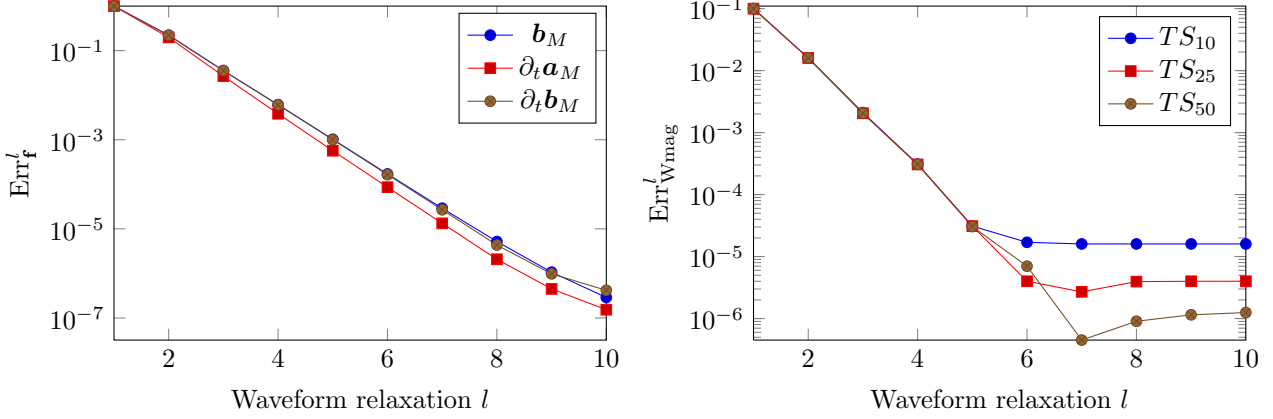


Figure 6: Left: Convergence of the macroscale waveforms for successive WR iterations (case with 1 time window and the same time discretization at the macroscale and the mesoscale). Right: Relative error on magnetic energy as a function of the WR iterations. The macroscale time grid comprise 10, 25 and 50 time steps per period, respectively whereas the time grid for the mesoscale problems comprise 50 time steps per period. In both cases, a macroscale mesh with 8722 elements with 25 elements for the homogenized domain was used. The relative error between the reference and the monolithic plots is 0.01243.

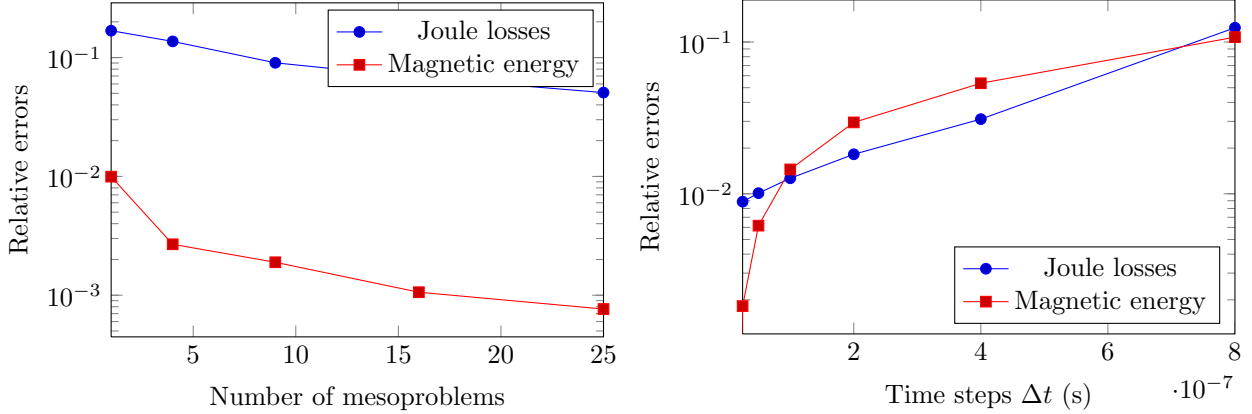


Figure 7: Relative errors on eddy current losses and magnetic energy between the waveform relaxation and the reference cases. Left: Relative errors as a function of the number of mesoproblems (1 to 25 mesoproblems are considered for the homogenized domain). Right: Relative errors as a function of the time discretization. The time step ranges from $2.5 \cdot 10^{-8}$ s to $8 \cdot 10^{-7}$ s.

value, smaller errors are even obtained for finer macroscale time grids. This underlines the possibility for efficient and consistent usage of multirate time stepping

Figure 7 depicts the convergence of the eddy current losses and the magnetic field to the reference solutions when the spatial grid and time grid are refined. As can be seen in Figure 7 - left, the relative errors decrease as the number of mesoproblems is increased from 1 to 25. One Gauss point was considered for each element and therefore the macroscale mesh for the homogenized domain contains the same number of elements. Figure 7 - right depicts the same evolution for the case for different time discretizations. In this case, a linear convergence is observed for the eddy current losses (with the time derivative) whereas the curve for magnetic energy exhibits a faster convergence. A good agreement was also observed in the case of many time windows.

An empirical comparison of the computational cost between the two methods can be made on the basis of the formula (7.10). In our numerical computations, we have always found that the errors on eddy currents losses and on the magnetic energy ($\text{Err}_{\tau_P}^l$ and $\text{Err}_{W_{\text{mag}}}^l$) become smaller than the errors between monolithic and the reference quantities already at the third waveform relaxation iteration (see Table 2). The first iteration is not computationally costly as it involves the initialization of the mesoscale solution to zero. Therefore, it is reasonable to assume that the errors of both methods become comparable for

$N_{\text{WR}} = 2$. Neglecting the mesoscale costs related to the reading and the updating of the homogenized constitutive law (i.e.: $\kappa \rightarrow 0$) and considering $N_{\text{NR}}^{\text{m}} = 3$ for a residue of 10^{-6} so that $N_{\text{NR}}^{\text{m}} = N_{\text{NR}}^{\text{M}}$, then $N_{\text{WR}} < N_{\text{NR}}^{\text{M}} N_{\text{dim}}^{\text{m}}$ with $N_{\text{WR}} = 2$, $N_{\text{NR}}^{\text{M}} = 3$, $N_{\text{dim}}^{\text{m}} = 4$ for a three-dimensional problem (resp. $N_{\text{dim}}^{\text{m}} = 3$ for a two-dimensional problem) and a theoretical speed-up of 4.5 for two-dimensional problems (resp. 6 for three-dimensional problems) can be gained. However, the current proof-of-concept implementation only allows a speed up of 2.

9. Conclusion

In this paper the heterogeneous multiscale method was combined with the waveform relaxation method. An efficient algorithm exploiting exact Jacobian information based on Schur-complements was proposed. Estimates have shown that an optimal implementation of the algorithm can be expected to be up to 6 times faster than a comparably monolithic approach. In the case of multirate behavior, even higher speed-up are expected. Convergence and efficiency have been numerically investigated using a challenging test example. Finally, optimization of our implementation and applying the available convergence analysis of waveform relaxation for higher index differential algebraic systems is subject of future research.

Acknowledgment

This work was supported by the German Funding Agency (DFG) by the grant ‘Parallel and Explicit Methods for the Eddy Current Problem’ (SCHO-1562/1-1), the ‘Excellence Initiative’ of the German Federal and State Governments and the Graduate School CE at Technische Universität Darmstadt and the Belgian Science Policy under grant IAP P7/02 (Multiscale modelling of electrical energy system).

References

- [1] W. E, B. Engquist, Heterogeneous multiscale methods, *Communications in Mathematical Sciences* 1 (1) (2003) 87–132.
- [2] I. Niyonzima, R. Sabariego, P. Dular, F. Henrotte, C. Geuzaine, Computational homogenization for laminated ferromagnetic cores in magnetodynamics, *IEEE Transactions on Magnetics* 49 (5) (2012) 2049–2052.
- [3] I. Niyonzima, Multiscale finite element modeling of nonlinear quasistatic electromagnetic problems, Ph.D. thesis, Université de Liège – Belgium (September 2014).
- [4] O. Bottauscio, A. Manzini, Comparison of multiscale models for eddy current computation in granular magnetic materials, *Journal of Computational Physics* 253 (2013) 1–17.
- [5] J. K. Jacob K. White, F. Odeh, A. L. Sangiovanni-Vincentelli, A. E. Ruehli, Waveform relaxation: Theory and practice, Technical Report UCB/ERL M85/65, University of California, Berkley (1985).
- [6] S. Schöps, H. De Gersem, A. Bartel, A cosimulation framework for multirate time-integration of field/circuit coupled problems, *IEEE Transactions on Magnetics* 46 (2010) 3233–3236.
- [7] J. D. Jackson, *Classical electrodynamics*, 3rd Edition, John Wiley & Sons, 1998.
- [8] K. Schmidt, O. Sterz, R. Hiptmair, Estimating the eddy-current modeling error, *IEEE Transactions on Magnetics* 44 (6) (2008) 686–689.
- [9] A. Bossavit, *Computational Electromagnetism. Variational Formulations, Complementarity, Edge Elements*, Academic Press, 1998.
- [10] J. Brauer, Simple equations for the magnetization and reluctivity curves of steel, *IEEE Transactions on Magnetics* 11 (1) (1975) 81.
- [11] R. R. R., Représentation algébrique des caractéristiques magnétiques, *Bulletin de la Société Française des Electriciens - Tome VI* 5 (69) (1936) 881–892.
- [12] F. Bachinger, U. Langer, J. Schöberl, Numerical analysis of nonlinear multiharmonic eddy current problems, *Numerische Mathematik* 100 (4) (2005) 593–616.
- [13] A. Abdulle, Numerical homogenization methods for parabolic monotone problems, MATHICSE Technical Report 33.2015, EPFL, Lausanne (2015).
- [14] H. Brezis, *Functional analysis, Sobolev spaces and partial differential equations*, Springer Science & Business Media, 2010.
- [15] A. Visintin, Electromagnetic processes in doubly-nonlinear composites, *Communications in Partial Differential Equations* 33 (2008) 804–841.
- [16] A. Bensoussan, J.-L. Lions, G. Papanicolaou, *Asymptotic Analysis for Periodic Structures*, American Mathematical Society, 2011.
- [17] A. Visintin, Homogenization of doubly-nonlinear equations, *Rendiconti Lincei - Matematica E Applicazioni* 17 (2006) 211–222.
- [18] P. Henning, M. Ohlberger, A Newton-scheme framework for multiscale methods for nonlinear elliptic homogenization problems, in: *Proceedings of the Conference Algoritmy*, 2015, pp. 65–74.
- [19] V. Barbu, *Nonlinear semigroups and differential equations in Banach spaces*, Leyden-Noordhoff, 1976.
- [20] H. Brezis, *Opérateurs maximaux monotones et semi-groupes de contractions dans les espaces de Hilbert*, North-Holland, Amsterdam, 1973.

- [21] F. E. Browder, Existence theorems for nonlinear partial differential equations, in: Proc. Sympos. Pure Math, Vol. 16, 1970, pp. 1–60.
- [22] A. Abdulle, G. Vilmart, Coupling heterogeneous multiscale FEM with Runge–Kutta methods for parabolic homogenization problems: A fully discrete spacetime analysis, *Mathematical Models and Methods in Applied Sciences* 22 (06) (2012) 1250002/1–1250002/40.
- [23] R. Grb, M. Gnther, U. Wever, Q. Zheng, Optimization of parallel multilevel-Newton algorithms on workstation clusters, in: Euro-Par’96 Parallel Processing, 1996, pp. 91–96.
- [24] A. Abdulle, M. E. Huber, V. Gilles, Linearized numerical homogenization method for nonlinear monotone parabolic multiscale problems, *Multiscale Modeling & Simulation* 13 (3) (2015) 916–952.
- [25] M. J. Gander, Waveform relaxation, in: *Encyclopedia of Applied and Computational Mathematics*, Springer, 2012.
- [26] M. Arnold, M. Günther, Preconditioned dynamic iteration for coupled differential-algebraic systems, *BIT Numerical Mathematics* 41 (1) (2001) 1–25.
- [27] E. Lelarasmee, A. E. Ruehli, A. L. Sangiovanni-Vincentelli, The waveform relaxation method for time-domain analysis of large scale integrated circuits, *IEEE Transactions on Computer-Aided Design of Integrated Circuits and Systems* 1 (3) (1982) 131–145.
- [28] K. Burrage, *Parallel and sequential methods for ordinary differential equations*, Oxford University Press, Oxford, 1995.
- [29] U. Miekala, O. Nevanlinna, Convergence of dynamic iteration methods for initial value problems, *SIAM Journal on Scientific Computing* 8 (1987) 459–482.
- [30] M. L. Crow, M. D. Ilic, The waveform relaxation method for systems of differential/algebraic equations, *Mathematical and Computer Modelling* 19 (12) (1994) 67–84.
- [31] A. Bartel, M. Brunk, M. Günther, S. Schöps, Dynamic iteration for coupled problems of electric circuits and distributed devices, *SIAM Journal on Scientific Computing* 35 (2) (2013) B315–B335.
- [32] J.-L. Lions, Y. Maday, G. Turinici, A parareal in time discretization of PDE’s, *Comptes Rendus de l’Académie des Sciences - Series I - Mathematics* 332 (2001) 661–668.
- [33] M. J. Gander, S. Vanderwalle, Analysis of the parareal time-parallel time-integration method, *SIAM Journal on Scientific Computing* 29 (2) (2007) 556–578.
- [34] M. Astorino, F. Chouly, A. Quarteroni, Multiscale coupling of finite element and lattice Boltzmann methods for time dependent problems, *MOX–Report 47/2012*, Politecnico di Milano (2012).
- [35] E. Hairer, G. Wanner, *Solving Ordinary Differential Equations: Stiff and differential-algebraic problems*, Springer Verlag, 2010.
- [36] P. Dular, C. Geuzaine, F. Henrotte, W. Legros, A general environment for the treatment of discrete problems and its application to the finite element method, *IEEE Transactions on Magnetics* 34 (5) (1998) 3395–3398.